NAVAL POSTGRADUATE SCHOOL
Monterey, California

THESIS

PROCESSING, MICROSTRUCTURE AND
SUPERPLASTICITY IN Al-Mg-Mn ALLOYS

by

Chris D. Meyer

DECEMBER 1991

Thesis Advisor: Terry R. McNelley

Unclassified

SECURITY CLASSIFICATION OF THIS PAGE

REPORT DOCUMENTATION PAGE

Form Approved OMB No 0704-0188

1a. REPORT SECURITY CLASSIFICATION: Unclassified	1b. RESTRICTIVE MARKINGS
2a. SECURITY CLASSIFICATION AUTHORITY	3. DISTRIBUTION/AVAILABILITY OF REPORT: Approved for public release: Distribution is unlimited
2b. DECLASSIFICATION/DOWNGRADING SCHEDULE	
4. PERFORMING ORGANIZATION REPORT NUMBER(S)	5. MONITORING ORGANIZATION REPORT NUMBER(S)
6a. NAME OF PERFORMING ORGANIZATION: Naval Postgraduate School; 6b. OFFICE SYMBOL (If applicable): ME	7a. NAME OF MONITORING ORGANIZATION: Naval Postgraduate School
6c. ADDRESS (City, State and ZIP Code): Monterey, CA 93943-5000	7b. ADDRESS (City, State, and ZIP Code): Monterey, CA 93943-5000
8a. NAME OF FUNDING/SPONSORING ORGANIZATION; 8b. OFFICE SYMBOL (If applicable)	9. PROCUREMENT INSTRUMENT IDENTIFICATION NUMBER
8c. ADDRESS (City, State, and ZIP Code)	10. SOURCE OF FUNDING NUMBER: PROGRAM ELEMENT NO. / PROJECT NO. / TASK NO. / WORK UNIT ACCESSION NO.

11. TITLE (Include Security Classification)

PROCESSING, MICROSTRUCTURE AND SUPERPLASTICITY IN Al-Mg-Mn ALLOYS

12. PERSONAL AUTHORS

CHRIS D. MEYER

13a. TYPE OF REPORT	13b. TIME COVERED	14. DATE OF REPORT (Year, Month, Day)	15. PAGE COUNT
Master's Thesis	FROM_____ TO_____	DECEMBER 1991	73

16. SUPPLEMENTARY NOTATION

The views expressed are those of the author and do not reflect the official policy or position of the Department of Defense or the U.S. Government

17. COSATI CODES			18. SUBJECT TERMS (Continue on reverse if necessary and identify by block numbers)
FIELD	GROUP	SUB-GROUP	superplasticity, particle stimulated nucleation

19. ABSTRACT (Continue on reverse if necessary and identify by block numbers)

A thermomechanical processing (TMP) schedule developed in previous work was modified to provide for an increasing strain and strain rate with each rolling pass. Three alloys, Al-10Mg, Al-10Mg-0.2Mn, and Al-10Mg-0.5Mn (compositions in wt. pct.), were processed utilizing this schedule. Samples were obtained following various rolling passes for subsequent microscopy analysis. Materials in both the as-rolled condition and following 25 minutes of annealing were studied. Utilizing backscattered imaging techniques with the scanning electron microscope, the microstructural evolution of these alloys during the TMP was studied. Second phase particles were observed to precipitate on grain boundaries and deformation structures in the intermediate stages of the TMP. In addition, second phase precipitates developed on $MnAl_6$ particles through heterogeneous nucleation in the Manganese containing alloys. Particle stimulated nucleation of recrystallization was observed in the latter stages of the TMP as precipitate particles coarsened. Tensile testing at 300°C demonstrated the superplastic response of each alloy, and showed that the addition of Manganese enhances superplastic response. Strain rate sensitivity coefficients were observed to initially decrease with increasing strain, but then increased with further straining.

20. DISTRIBUTION/AVAILABILITY OF ABSTRACT	21. ABSTRACT SECURITY CLASSIFICATION
XX UNCLASSIFIED/UNLIMITED __ SAME AS RPT __ DTIC USERS	unclassified

22a. NAME OF RESPONSIBLE INDIVIDUAL	22b. TELEPHONE (Include Area Code)	22c. OFFICE SYMBOL
Terry R. McNelley	(408) 646-2589	ME/Mc

DD Form 1473, JUN 86 *Previous editions are obsolete.* S/N 0102-LF-014-6603

SECURITY CLASSIFICATION OF THIS PAGE Unclassified

Approved for public release: Distribution is unlimited

Processing, Microstructure and Superplasticity in Al-Mg-Mn Alloys

by

Chris D. Meyer
Lieutenant, United States Navy
B.S., Civil Engineering, Marquette University, 1986

Submitted in partial fulfillment of the
requirements for the degree of

MASTER OF SCIENCE
IN ENGINEERING SCIENCE

from the

NAVAL POSTGRADUATE SCHOOL

DECEMBER 1991

Author: 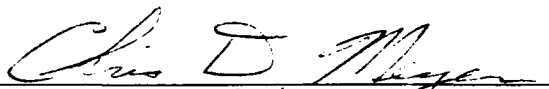
Chris D. Meyer

Approved by: 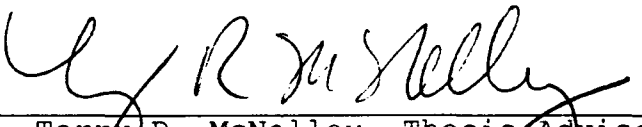
Terry R. McNelley, Thesis Advisor

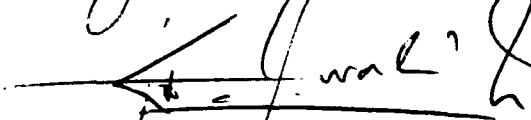
Peter N. Kalu, Second Reader


A.J. Healey, Chairman
Department of Mechanical Engineering

ABSTRACT

A thermomechanical processing (TMP) schedule developed in previous work was modified to provide for an increasing strain and strain rate with each rolling pass. Three alloys, Al-10Mg, Al-10Mg-0.2Mn, and Al-10Mg-0.5Mn (compositions in wt. pct.), were processed utilizing this schedule. Samples were obtained following various rolling passes for subsequent microscopy analysis. Materials in both the as-rolled condition and following 25 minutes of annealing were studied. Utilizing backscattered imaging techniques with the scanning electron microscope, the microstructural evolution of these alloys during the TMP was studied. Second phase particles were observed to precipitate on grain boundaries and deformation structures in the intermediate stages of the TMP. In addition, second phase precipitates developed on $MnAl_6$ particles through heterogeneous nucleation in the Manganese containing alloys. Particle stimulated nucleation of recrystallization was observed in the latter stages of the TMP as precipitate particles coarsened. Tensile testing at 300°C demonstrated the superplastic response of each alloy, and showed that the addition of Manganese enhances superplastic response. Strain rate sensitivity coefficients were observed to initially decrease with increasing strain, but then increased with further straining.

TABLE OF CONTENTS

LIST OF TABLES

LIST OF FIGURES

ACKNOWLEDGEMENTS

I would like to express my sincere thanks to Professor Terry McNelley for his expert advice and kind help in guiding me to completion of this research. Also, a special thanks to Doctors Peter Kalu and Roy Crooks for helping me to unlock some of the mysteries of this work. I would also like to thank Miss Elisabeth Grayson, Mr. Tom McCord, and LCDR Mike Coleman for their support. Finally, I would like to thank my fiance, Sue, for giving me a light at the end of the tunnel.

I. INTRODUCTION

Superplasticity is the ability of a material to undergo large, tensile plastic deformation. Tensile elongations greater than 200% are considered superplastic, and elongations as large as 1000% are not uncommon. Because of these high ductilities, complex shapes can be fabricated from single pieces of sheet metal. The resulting reduction in fasteners reduces weight. Also, stress concentrations are reduced, and thus susceptibility to fatigue and corrosion is lessened. These features have been particularly appealing to aircraft designers, and there is now a substantial market in the aircraft industry for superplastically fabricated components. These alloys are also finding their way into the shipboard environment. Current applications of superplasticity in the marine industry include the manufacture of fire-control radar dishes as single components and two-piece compass stabilizer units. Other applications are likely to follow.

Initially, it was thought that only eutectic alloys, such as Pb-Sn, were capable of superplasticity. Since such low strength alloys have no structural uses, the phenomenon was not widely explored. Work in the Soviet Union investigated superplastic properties in a wide range of alloys [Ref. 1]. Interest in this topic in the West was heightened after Underwood's 1962 review [Ref. 2] of

the Soviet research. In the 1970's it was established that superplasticity could be induced in a variety of Titanium, steel, and Aluminum alloys which also have useful commercial properties. Today, Aluminum-Copper-Zirconium alloys (SUPRAL) are the most commonly used superplastic Aluminum alloys. Other Aluminum alloys can be processed to give superplastic response, notably the high strength alloy 7475. It has been seen that such alloys require close attention to thermomechanical processing (TMP) parameters and alloy content to produce the requisite microstructure for superplastic deformation.

Recent work in this area at the Naval Postgraduate School (NPS) has focused on superplasticity in Aluminum-Magnesium alloys at 300°C. Ductilities exceeding 1100% have been reported at this temperature [Ref. 3]. It has been demonstrated that the superplastic response is very sensitive to TMP parameters [Refs. 4, 5]. The purpose of this research is to identify the microstructural evolution of high Magnesium, Aluminum-Magnesium-Manganese alloys during TMP, and to show the effects of this evolution on superplastic response.

II. BACKGROUND

Superplastic deformation can only be accomplished within certain ranges of temperature and strain rate. Generally, temperatures of approximately 0.5 - 0.65T_m are considered necessary for superplastic flow. Such temperatures reflect the role of diffusion in the process of superplastic flow. In addition, several microstructural requirements must be met. First, the material must have a fine grain size, typically less than 10 μm. Also, the presence of a second phase is usually required to stabilize the microstructure and prevent grain growth during straining. Further, it is believed that an equiaxed structure is necessary to allow grain boundary sliding and associated grain rotation during deformation. Finally, grain boundaries must resist tensile separation while supporting grain boundary sliding [Ref. 6].

Materials possessing these microstructural characteristics will be inherently strain rate sensitive at superplastic deformation temperatures. This sensitivity is usually described by the strain rate sensitivity coefficient, m, from

$$\sigma = K\dot{\epsilon}^m \qquad (1)$$

where σ is the flow stress, K is a material constant and $\dot{\epsilon}$ is the strain rate [Ref. 7]. Typical values of m for superplastic materials range from m = 0.4 to 0.5 and sometimes

higher still. Resistance to localized necking, critical to superplastic flow, is increased with increasing m-values.

Although many details of superplastic flow are not fully understood, the mechanism can be descrided phenomologically in terms of a power law relation between grain size, temperature, and strain rate. Recognizing that there is also a contribution to superplastic flow by dislocation creep, the total deformation rate can be written as the sum of two terms,

$$\dot{\epsilon}_t = \dot{\epsilon}_{d.c.} + \dot{\epsilon}_s \qquad (2)$$

where $\dot{\epsilon}_t$ is the total deformation rate, $\dot{\epsilon}_{d.c.}$ is the deformation rate due to dislocation creep, and $\dot{\epsilon}_s$ is the deformation rate due to superplastic flow [Ref. 3]. Considering only glide-controlled creep, and superplastic deformation by slip-accommodated grain boundary sliding, Equation (2) can be rewritten as

$$\dot{\epsilon}_t = KD_s\left(\frac{\sigma}{E}\right)^3 + AD_{eff}\left(\frac{1}{d}\right)^2 \left(\frac{\sigma}{E}\right)^2 \qquad (3)$$

where K and A are constants, D_s is the solute diffusion coefficient for Magnesium in Aluminum, E is Young's modulus, D_{eff} is the effective diffusion coefficient, and d is the average grain size [Ref. 3]. The influence of temperature in this equation is realized through the two diffusion coefficients.

The first term in Equation (3) is independent of grain size, while the second term has an inverse dependency on grain

size. Thus a small grain size will result in the second term being much larger than the first term, and in this instance the total strain rate will depend upon σ^2. That is, the m value in Equation (1) will tend toward m = 0.5 if d remains constant. For large values of d, the superplastic strain rate, represented by the second term, will be smaller than the dislocation creep strain rate represented by the first term. In this case the total strain rate will depend upon σ^3, and m will tend toward values of 0.3. However, at superplastic deformation temperatures, grain size is not stable. If a fine grain size has been achieved through TMP, grain growth during deformation may result in an initially large value of m decreasing as strain increases. This may be especially true at low strain rates, where there is more time at temperature during straining. This idea has been used to describe the decrease in m value with increasing strain in an Aluminum-Magnesium-Zirconium alloy for strains up to ε = 0.5 in. [Ref. 8]

Thermomechanical processing is employed to achieve the required microstructure for superplastic forming. Specifically, the goal of the TMP is to produce a fine recrystallized grain structure in the material. The first research at NPS focused on identifying proper TMP parameters to achieve superplastic response [Ref. 9]. Subsequent research indicated that the strain rate sensitivity coefficient is maximum at the initial stages of straining, and

decreases to m ≈ 0.3 with further straining. This behavior suggested a transformation in deformation mechanism from one of grain boundary sliding to one of dislocation glide-control at the lower m value [Ref. 8]. Based on this information, the TMP schedule was modified with various interpass annealing times and temperatures. It became clear that the rolling reduction schedule combined with the time and temperature of interpass annealing combine in determining the extent of recrystallization [Ref. 10]. Adequate time at temperature between rolling passes now seems to be required to allow for the appropriate precipitation and recrystallization reactions to occur. Although the exact mechanisms for these reactions are not known, particle stimulated nucleation (PSN) of recrystallization has been identified as the likely mechanism [Ref. 11].

III. EXPERIMENTAL PROCEDURE

A. CASTING AND SECTIONING

The Alcoa Technical Center, Alcoa Center, Pennsylvania, provided three direct- chill cast ingots designated S572824, S572825, and 501300A. These ingots measured 6 in. diameter x approximately 23 in. length (150 mm dia. x 580 mm length). Nominal compositions of each of these alloys are presented in Table I.

TABLE I. NOMINAL ALLOY COMPOSITIONS (wt%)

CASTING #	Mg	Mn	Si	Fe	Ti	Be	Al
S572824	10.1	0.00	0.01	0.02	0.01	0.0004	Balance
S572825	10.0	0.22	0.01	0.02	0.01	0.0003	Balance
501300A	10.2	0.52	0.01	0.03	0.01	0.0002	Balance

The ingots were sectioned into billets measuring 3.75 in. x 1.25 in x 1.25 in (93.5 mm x 31.8 mm x 31.8 mm) for the Al-10Mg and Al-10Mg-0.2Mn alloys, and billets measuring 3.00 in x 1.0 in x 1.0 in (76.2 mm x 25.4 mm x 25.4 mm) for the Al-10Mg-0.5Mn alloy. The long dimension of the billets conformed to the longitudinal axis of the castings.

B. THERMOMECHANICAL PROCESSING

Figure 1 is a schematic representation of the TMP employed in this study. The schedule essentially consists of two parts. The first part consists of homogenization and hot working. The billets were given an initial solution treatment in a Lindberg, Model 51828 furnace for 6 hours at 440°C. This temperature is just below the eutectic temperature of 451°C, thus avoiding melting any non-equilibrium initially present. The second part is warm rolling done below the Mg solvus temperature. Homogenization was completed by an additional 18 hours at 500°C. The billets were then upset forged along the longitudinal axis on a Baldwin - Tate - Emery testing machine with platens heated to 440°C. The final thickness after forging was 1.00 in (25.4 mm) ±0.05 in (1.27 mm). The forged billets were then reheated at 500°C for 1 hour to ensure that subsequent quenching was done from above the solvus temperature. The fully homogenized forgings were then given a vigorous oil quench for 1 minute.

The second part of the TMP (Figure 1) consists of warm rolling at 300°C, a temperature below the **B**-phase solvus temperature of 360°C [Ref. 12]. The warm rolling is intended to develop a refined microstructure necessary for superplasticity. Previous work has shown that the superplastic response of a material is a sensitive function of the warm rolling parameters. These parameters are: the rolling temperature, the rolling reduction (strain) per pass, the

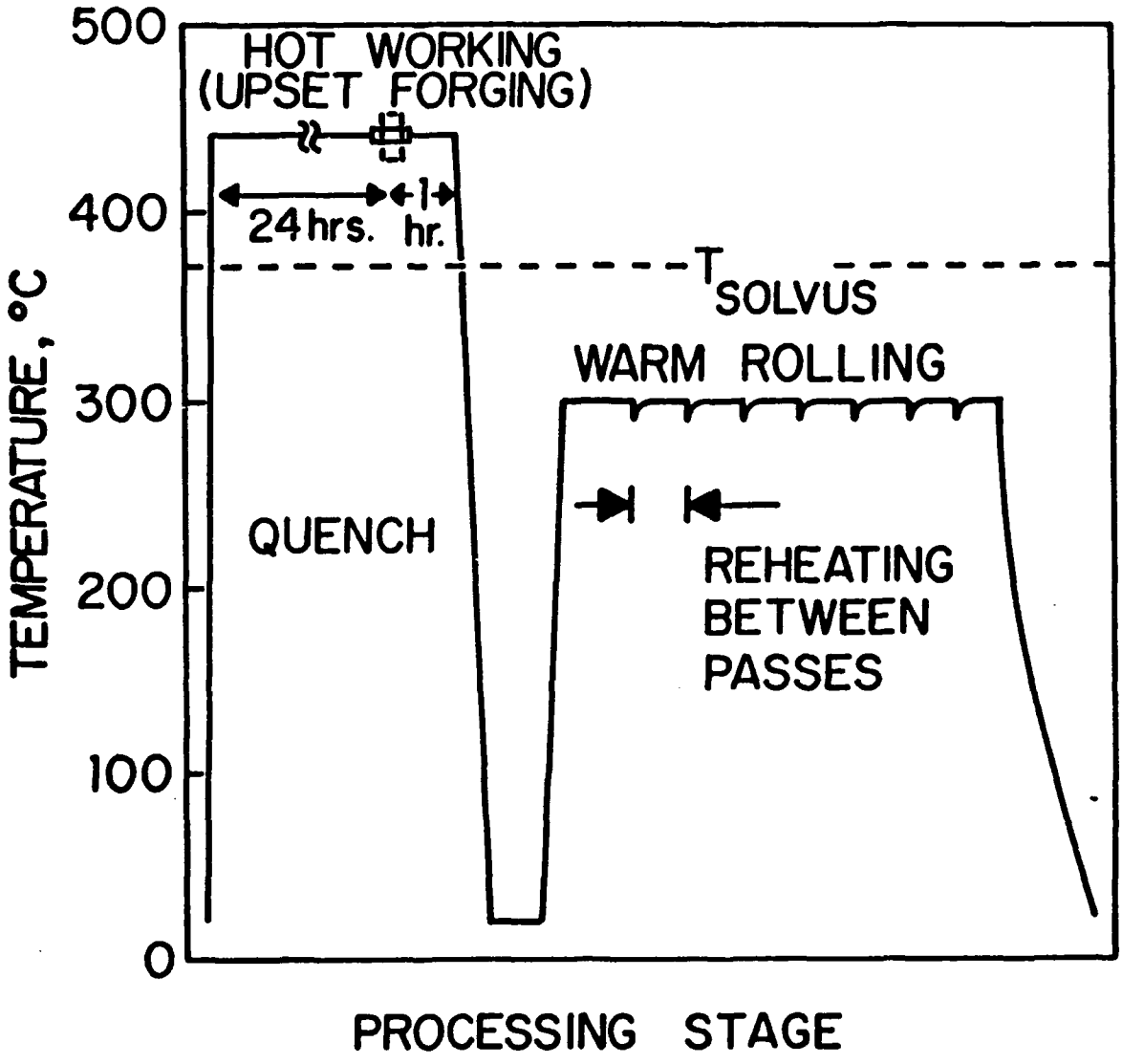

Figure 1. Thermomechanical Processing Schedule. Homogenization and Quenching, Followed by 12 Rolling Passes With a 30 Minute Anneal at 300°C Between Each Pass.

strain rate per pass, the reheating temperature, the duration of the reheating interval, and the total strain accumulated.

alloys, the rolling temperature and reheating temperature have both been 300°C.

The research by Gorsuch [Ref. 13] was concerned with the effect of the duration of reheating between passes on a given rolling schedule. The schedule, developed by Gorsuch, is presented in Table II. Strain and strain rate in this schedule were calculated on the basis of a constant reduction per pass through the first 7 passes. The subsequent changes in reduction reflect the need to remain within the rolling mill's capabilities. Gorsuch followed this schedule by adjusting the mill gap at each pass to correspond to the listed values of Δh. He did not measure the sample dimensions after each pass and so the values of strain and strain rate do not reflect springback in the mill. It should be noted that the calculated values of strain increase through the first 7 passes but then decrease on pass 8. The strain then increases again through pass 11 and, finally, decreases at the final pass. The recrystallized grain size generally decreases as the prior strain increases. Hence it was decided to modify this schedule so that both strain and strain rate always increase on each successive pass. Such a schedule might be expected to produce greater refinement when compared to one involving only a small strain on the final pass. Equations (4) and (5), were used to modify the Gorsuch schedule:

TABLE II. ROLLING SCHEDULE OF GORSUCH

PASS #	h_i (in)	Δh (in)	ε_p (%)	$\dot{\varepsilon}_p$ (s^{-1})
1	0.94	0.10	10.6	0.950
2	0.84	0.10	11.9	1.068
3	0.74	0.10	13.5	1.216
4	0.64	0.10	15.6	1.413
5	0.54	0.10	18.5	1.687
6	0.44	0.10	22.7	2.091
7	0.34	0.10	29.4	2.750
8	0.24	0.06	25.0	2.987
9	0.18	0.05	27.8	3.662
10	0.13	0.04	30.8	4.567
11	0.09	0.03	33.3	5.740
12	0.06	0.013	21.7	5.523

$$\varepsilon_p = \frac{h_i - h_f}{h_i} = \frac{\Delta h}{h_i} \tag{4}$$

$$\dot{\varepsilon}_p = \frac{2\pi Rn}{\sqrt{Rh_i}} \sqrt{\varepsilon} \left(1 + \frac{\varepsilon}{4}\right) \tag{5}$$

where ε_p is the strain associated with a rolling pass; $\dot{\varepsilon}_p$ is the strain rate; h_i and h_f are the initial and final thicknesses, respectively; h is the reduction; R is the radius of the rolls; and n is the speed of the rolls in rads/s. The schedule modification was accomplished by adjusting the distribution of reductions as shown in Table III. Essentially,

larger reductions are taken in passes 2-6 in order that adjustments can be made to later passes to prevent a decrease in $_p$ on successive passes. Note that the values of ε_p and $\dot{\varepsilon}_p$ now increase with each successive pass.

TABLE III. MODIFIED ROLLING SCHEDULE

PASS #	h_i (in)	Δh (in)	ε_p (%)	$\dot{\varepsilon}_p$ (s^{-1})
1	1.00	0.10	10.0	0.893
2	0.90	0.11	12.2	1.045
3	0.79	0.11	13.9	1.196
4	0.68	0.11	16.2	1.399
5	0.570	0.11	19.3	1.680
6	0.460	0.11	23.9	2.104
7	0.350	0.085	24.3	2.435
8	0.265	0.07	26.4	2.931
9	0.195	0.055	28.2	3.547
10	0.140	0.040	28.6	4.219
11	0.100	0.030	30.0	5.130
12	0.070	0.023	32.9	6.464

Prior to the start of rolling each forged and quenched alloy billet was placed in a Blue M, Model 8655-3 furnace and heated at 300°C for 30 minutes. Rolling was done using a Fenn Laboratory Rolling Mill. The mill gap settings were set by hand and checked with gage blocks prior to each pass. The gage blocks were specially made to conform to the rolling schedule and were accurate to ±0.001 in (0.025 mm). This method of

setting and checking the roll gaps ensured that each alloy was rolled in exactly the same way. Silicone spray lubricant was applied to the rolls prior to each pass beginning with pass 6, as it was at this point that mill stalling due to friction effects appeared to become a possibility. The rolled sheets were annealed at 300°C for 30 minutes between each pass.

The thickness of each rolled sheet was measures using a digital micrometer immediately after each rolling pass. After passes 3,6,8,10, and 12 the sheet was secured with c-clamps to a steel anvil and a small sample was cut off the end with a hand-held bandsaw. The anvil was arranged so that the cut samples fell into an ice-water quench. Total time out of the furnace was about 15 seconds when no samples were cut, and about 45 seconds when samples were cut. The sheet was then returned to the furnace for the 30 minute interpass anneal. Each sample was cut in half. One half was retained to represent the as rolled condition, and the other was annealed for 25 minutes at 300°C. At the conclusion of rolling these materials were allowed to air cool.

The measured thickness data for the three alloys is presented in Tables IV, V, and VI. The values of initial and final thickness, h_i, and final thickness, h_f, are from direct sample measurement, and Δh was determined from these values. Springback was determined by subtracting the mill gap from h_f. Strain and strain rate values were evaluated using Equations (4) and (5). It can be seen in Tables IV, V, and VI that for

each alloy the strain rate per pass increases throughout the schedule, although more slowly than predicted. The strain per pass increases through pass 6, than reaches an essentially constant value of 22-25% in the later stages. For the Al-10Mg-0.2Mn and Al-10Mg-0.5Mn alloys, the strain at the last pass decreased slightly below this range. These decreases may reflect the cumulative effects of springback. However, it appears that this schedule does provide a basis for rolling with an essentially constant strain per pass in the later rolling passes.

TABLE IV. Al-10Mg ROLLING SCHEDULE

PASS	MILL GAP (in)	h_i (in)	h_f (in)	Δh (in)	SPRING-BACK (in)	ε_p (%)	$\dot{\varepsilon}_p$ (s^{-1})
1	0.900	1.005	0.936	0.069	0.036	6.68	0.732
2	0.790	0.936	0.821	0.115	0.031	12.29	1.029
3	0.680	0.821	0.715	0.106	0.035	12.91	1.128
4	0.570	0.715	0.602	0.113	0.032	15.80	1.346
5	0.460	0.602	0.501	0.101	0.041	16.78	1.515
6	0.350	0.501	0.389	0.112	0.039	22.36	1.943
7	0.265	0.389	0.299	0.090	0.034	23.14	2.248
8	0.195	0.299	0.232	0.067	0.037	22.41	2.519
9	0.140	0.232	0.172	0.060	0.032	25.86	3.097
10	0.100	0.172	0.134	0.038	0.034	22.09	3.295
11	0.070	0.134	0.104	0.030	0.034	22.39	3.760
12	0.047	0.104	0.078	0.026	0.031	25.00	4.538

TABLE V. Al-10Mg-0.2Mn ROLLING SCHEDULE

PASS	MILL-GAP (in)	h_i (in)	h_f (in)	Δh (in)	SPRING-BACK (in)	ε_p (%)	$\dot{\varepsilon}_p$ (s^{-1})
1	0.900	1.000	0.924	0.076	0.024	7.60	0.774
2	0.790	0.924	0.822	0.102	0.032	11.04	0.979
3	0.680	0.822	0.711	0.111	0.031	13.50	1.154
4	0.570	0.711	0.601	0.110	0.031	15.47	1.241
5	0.460	0.601	0.490	0.111	0.030	18.47	1.366
6	0.350	0.490	0.381	0.109	0.031	22.24	1.959
7	0.265	0.490	0.296	0.085	0.031	22.31	2.226
8	0.195	0.381	0.226	0.067	0.034	22.64	2.545
9	0.140	0.296	0.172	0.057	0.032	24.89	3.051
10	0.100	0.172	0.131	0.041	0.031	23.84	4.244
11	0.070	0.131	0.099	0.032	0.029	24.43	4.930
12	0.047	0.099	0.078	0.021	0.031	21.21	5.245

TABLE VI. Al-10Mg-0.5Mn ROLLING SCHEDULE

PASS	MILL GAP (in)	h_i (in)	h_f (in)	Δh (in)	SPRING -BACK (in)	ε_p (%)	$\dot{\varepsilon}_p$ (s^{-1})
1	0.900	1.000	0.940	0.060	0.040	6.00	0.691
2	0.790	0.940	0.824	0.116	0.034	12.34	1.036
3	0.680	0.824	0.715	0.109	0.035	13.22	1.149
4	0.570	0.715	0.607	0.108	0.037	15.10	1.325
5	0.460	0.607	0.499	0.108	0.039	17.79	1.572
6	0.350	0.499	0.391	0.108	0.041	21.64	1.927
7	0.265	0.391	0.312	0.079	0.047	20.20	2.098
8	0.195	0.312	0.234	0.078	0.039	25.00	2.643
9	0.140	0.234	0.179	0.055	0.039	23.50	2.948
10	0.100	0.179	0.134	0.045	0.034	25.14	3.497
11	0.070	0.134	0.104	0.030	0.034	22.39	3.795
12	0.047	0.104	0.084	0.020	0.037	19.23	4.403

C. TENSILE TESTING

Sheet-type tensile test samples were cut from each rolled sheet according to Figure 2. Tensile testing was done on an Instron Model 6027 testing machine. A Marshal Model 2232 clamshell furnace maintained a constant test temperature of 300°C. The samples were placed in preheated grips and given 45 minutes in the furnace to equilibrate at test temperature. Seven different constant crosshead speeds, giving a range of strain rates from 6.65×10^{-2} sec^{-1} to 6.30×10^{-5} sec^{-1}, were used. Each sample was pulled to failure.

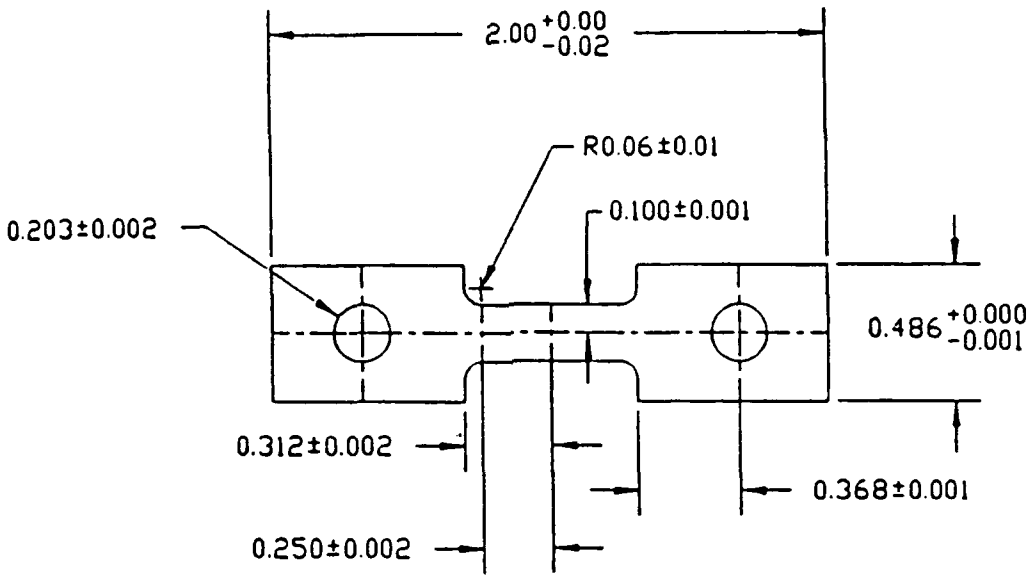

Figure 2. Tensile Test Specimen Design. Dimensions and Tolerances are in Inches.

D. DATA REDUCTION

A graph of load versus displacement was obtained from each test. This data was corrected to account for the elastic response of the testing machine, tightening of the grips, and the different crosshead speeds used in each test. The correction, outlined by Lee and McNelley [Ref. 9], allows data from all tests to be directly compared. This corrected data was then converted to plots of true stress versus true strain. Values of true stress were taken from these curves at calculated true strains of 0.02, 0.1, 0.2, 0.3, 0.5 and 1.0. These true stress values were plotted on double log axes

versus strain rate to determine the strain rate sensitivity coefficient, m, corresponding to strain value.

E. SCANNING ELECTRON MICROSCOPY

The samples cut from the rolling sheet during the intermediate stages of rolling were studied in a Cambridge, Model S200 scanning electron microscope. The backscattered imaging method was used. It was determined that backscattered imaging provided improved resolution of matrix structure, based on orientation contrast, over secondary imaging. In comparing Figure 3a, a secondary image, with Figure 3b, a backscattered image of the same field, it can be seen that the backscattered method provides more detail of matrix substructure.

Samples to be studied were not mounted for preparation. This practice avoided microstructural changes in the samples due to the heat of hot mounting and the stress of breaking the sample free of a cold mount. Mounted samples coated with a conductor do not give optimal results when using the backscattered imaging mode.

The samples were ground flat and polished using 1μ diamond paste. Following mechanical polishing, the samples were electropolished in a 10% hydrochloric acid- 90% butoxyethanol solution at 0°C. A voltage of 16VDC was applied for 3.5 minutes for the Al-10 Mg and Al-10Mg-0.2Mn alloys. A voltage

(a)

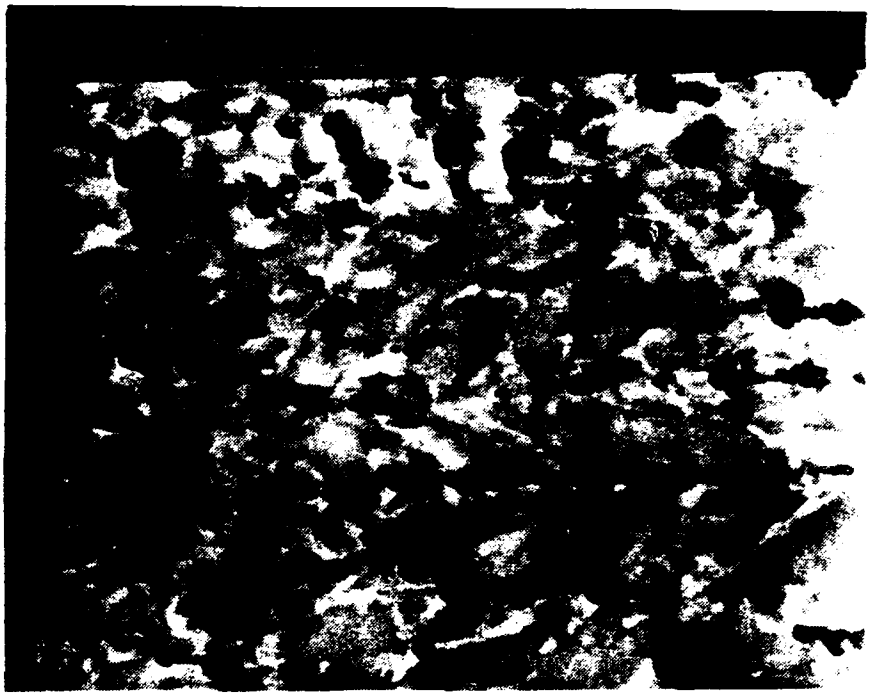

(b)

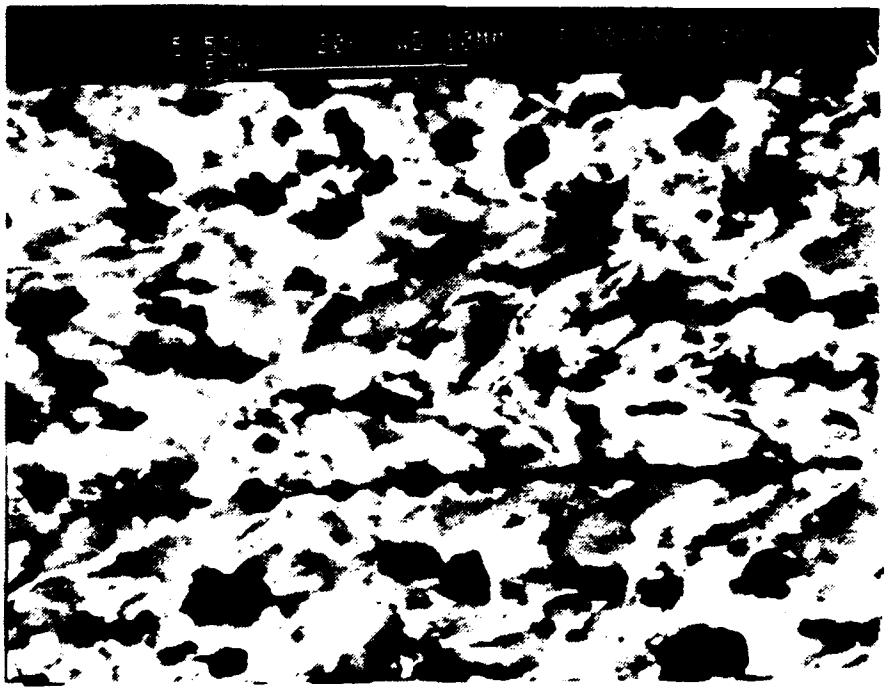

Figure 3. SEM Micrographs Showing the Same Field Utilizing: a.) Secondary Emission Imaging, and b.) Backscattered Imaging

of 19VDC was applied for 2 minutes for the Al-10Mg-0.5Mn alloy.

IV. RESULTS AND DISCUSSION

A. MICROSCOPY

Scanning electron microscopy of the samples obtained during the rolling processes allowed the microstructural evolution of each alloy to be studied. The microstructure of the Al-10Mg alloy is presented here following rolling passes 3, 6, 8, 10, and 12. Micrographs of both the as-rolled and the annealed (25 minutes at 300°C) conditions are shown in each case. The annealed condition essentially represents the microstructure at the start of the next rolling pass. Microscopy results for the Al-10Mg-0.2Mn and Al-10Mg-0.5Mn alloys are considered for rolling passes 3, 8, and 12 only, representing the initial, intermediate, and final stages of the microstructural evolution. Again, both the as-rolled and annealed microstructures for each of these stages will be presented. Accumulated rolling strains for the three alloys at each point of microstructural examination are shown in Table VII.

1. Al-10Mg

Typical microstructure of the as-rolled condition following pass 3 is presented in Figure 4-a. The microstructure shows clear evidence of precipitation of intermetallic β-phase on the grain boundaries from the prior

TABLE VII. ACCUMULATED ROLLING STRAINS (in/in)

PASS #	Al-10Mg	Al-10Mg	Al-10Mg
3	0.20	0.34	0.34
5	0.70	0.96	0.94
8	1.47	1.47	1.45
10	2.01	2.03	2.01
12	2.56	2.55	2.48

solid solution. Deformation bands and precipitation within grain interiors are also apparent. The pattern of precipitation within the grains suggests two possible precipitation sites. The first possibility is precipitation on deformation bands not imaged due to their orientation. The second possibility is precipitation on deformation bands from a previous rolling pass which were obliterated during subsequent rolling. A typical example of the structure following annealing is represented by Figure 4-b. The important feature to note is precipitation along the deformation band boundaries. It is also notable that evidence of recovery (shown by subgrain contrast within the matrix) is more pronounced after the annealing.

Figure 5-a represents the as rolled microstructure following pass 6. It is apparent (compare Figures 4-a and 5-a) that more precipitation has occurred since pass 3. Also the

(a)

(b)

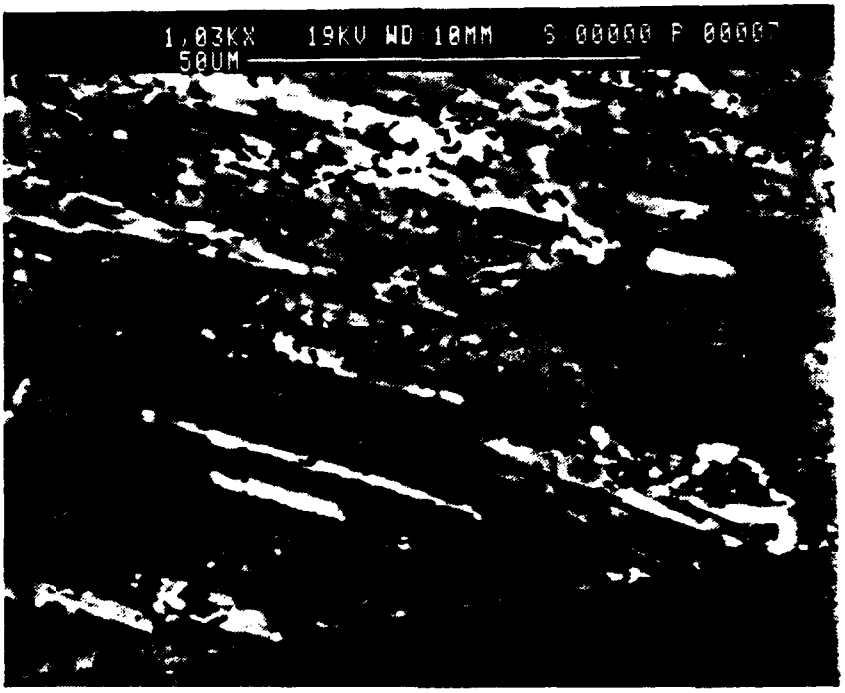

Figure 4. Backscattered SEM Micrograph Showing the Al-10Mg Alloy Following Rolling Pass 3: a.) In the As-rolled Condition, b.) Following 25 Minutes of Annealing at 300°C.

precipitates have increased in size. The alignment of the precipitates indicates precipitation along deformation bands. Contrast variations within the matrix suggest extensive recovery. The effect of annealing after pass 6 is shown in Figure 5-b. The precipitates do not appear to have coarsened during annealing and there is no evidence of recrystallization in the matrix.

A typical as-rolled microstructure following pass 8 is shown in Figure 6-a. More precipitation is evident compared with pass 6 (Figure 5-a, noting the magnification difference). Some large precipitates have now developed due to coarsening, and the matrix microstructure remains recovered. The microstructure is also becoming more refined, as long deformation bands evident in Figure 4-a are now much shorter. Following annealing (Figure 6-b) there is no further precipitate coarsening, and no evidence of matrix recrystallization.

Figure 7-a presents the as-rolled microstructure following pass 10. Some particle coarsening has occurred (Compare Figures 7-a and 6-a). There are indications of local lattice rotation in the vicinity of many large precipitates, as evidenced by the feathery localized contrast in the neighborhood of the these particles. After annealing (Figure 7-b), he microstructure shows the first evidence of recrystallization. Isolated instances of recrystallization have occurred around several of the larger particles.

(a)

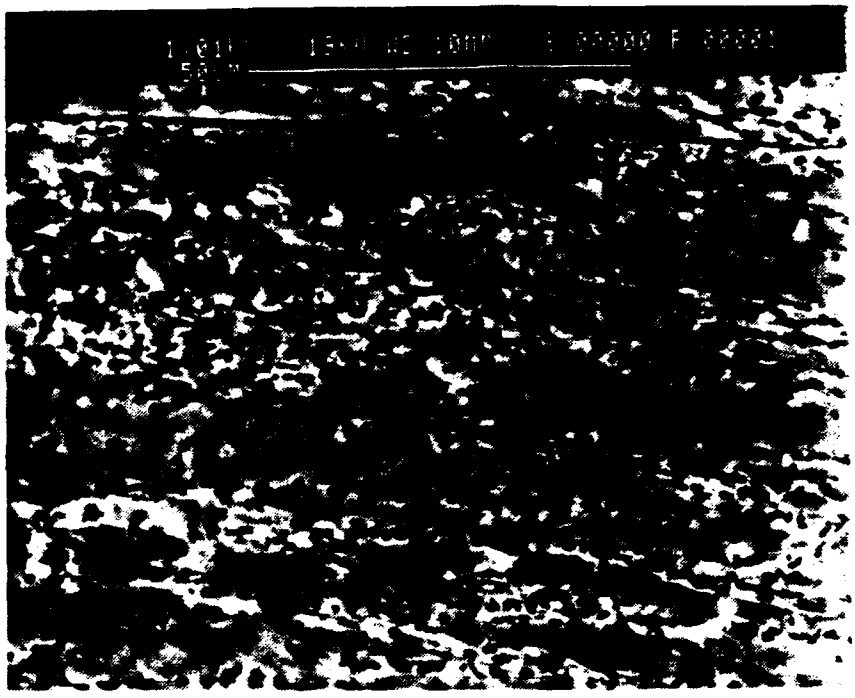

(b)

Figure 5. Backscattered SEM Micrograph Showing the Al-10Mg Alloy Following Rolling Pass 6: a.) In the As-rolled Condition, b.) Following 25 Minutes of Annealing at 300°.

(a)

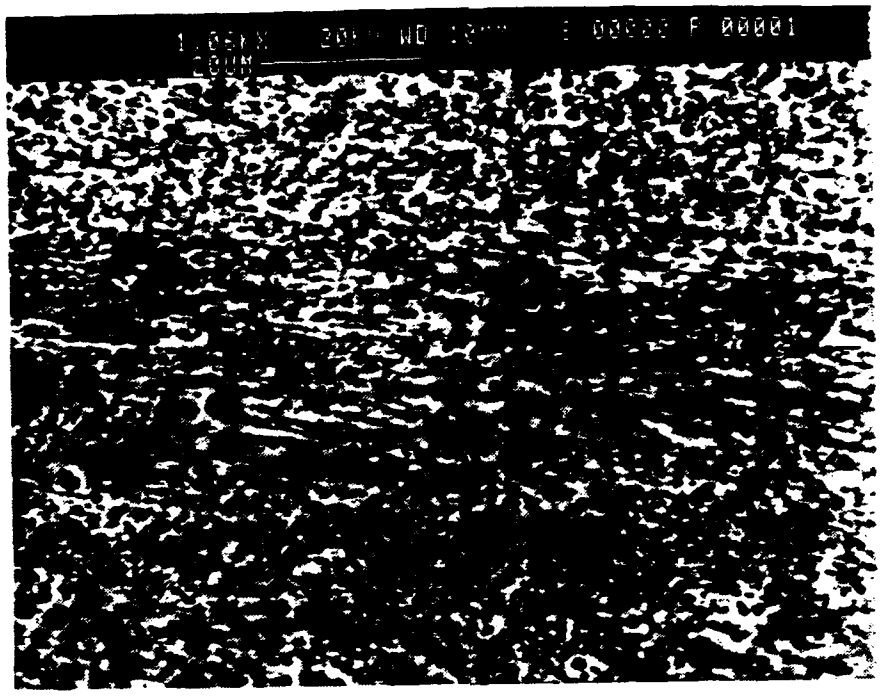

(b)

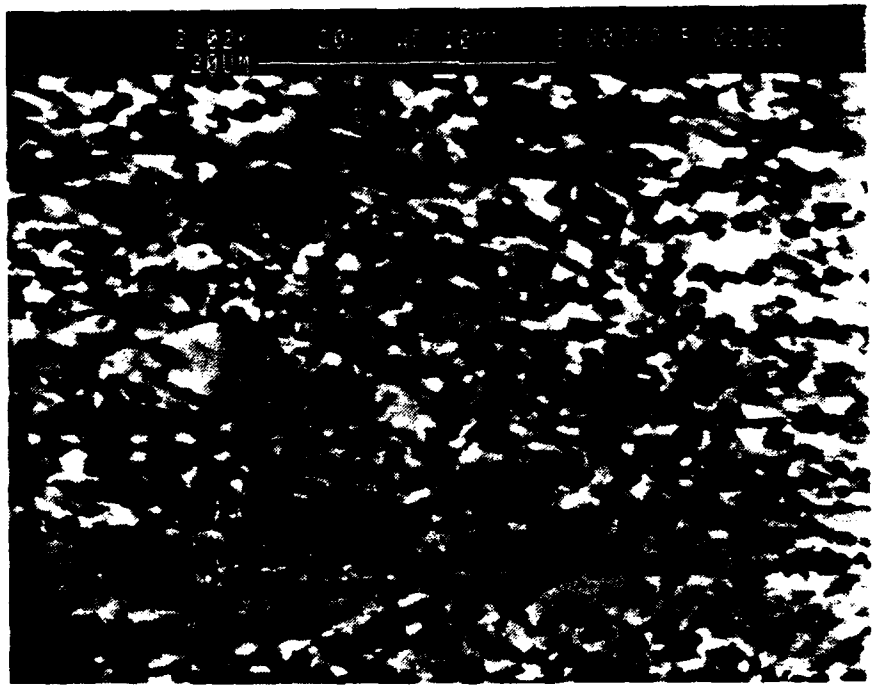

Figure 6. Backscattered SEM Micrograph Showing the Al-10Mg Alloy Following Rolling Pass 8: a.) In the As-rolled Condition, b.) Following 25 Minutes of Annealing at 300°C.

(a)

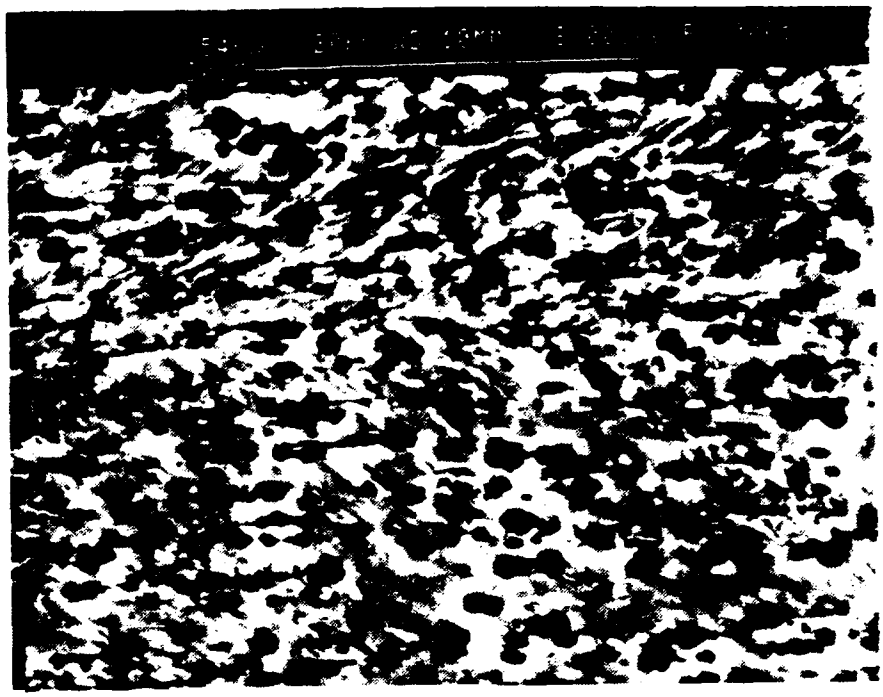

(b)

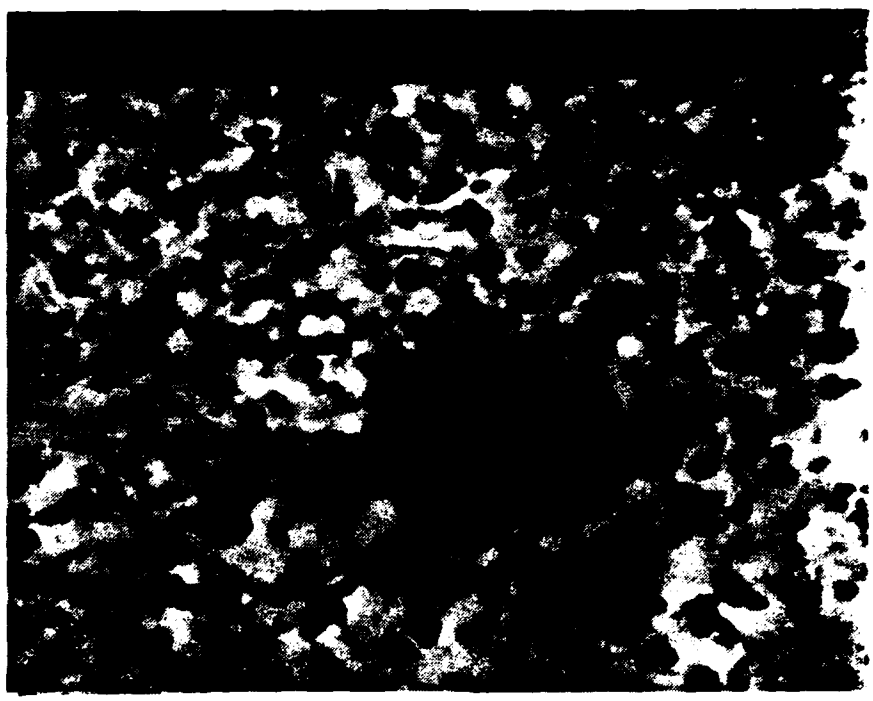

Figure 7. Backscattered SEM Micrograph Showing the Al-10Mg Alloy Following Rolling Pass 10: a.) In the As-rolled Condition, b.) Following 25 Minutes of Annealing at 300°C.

The microstructure following pass 12, the final rolling pass, is shown in Figure 8-a. The particles do not appear to have coarsened compared to pass 10. Some fine grains formed by recrystallization from previous passes can be discerned. Following annealing (Figure 8-b) the material in the fully processed condition exhibits some recrystallized grains associated with the larger particles. The extent of this recrystallization is greater than that seen in the microstructure following pass 10. However, the presence of some recovered regions within the matrix suggests that the material is not fully recrystallized. There appears to have been little or no particle coarsening during this annealing.

2. Al-10Mg-0.2Mn

Figure 9-a shows the effect of the Mn addition on the microstructure. In the as-rolled condition following pass 3 there is a substantial increase in the amount of precipitation when compared with the binary material (Compare Figures 9-a and 4-a). Extensive precipitation has occurred at prior grain boundaries and within the grains. Note that light colored particles, $MnAl_6$, have also precipitated. The $MnAl_6$ particles appear to serve as heterogeneous nucleation sites within grain interiors for β-phase precipitation. It can also be seen that many of these $MnAl_6$ particles have an elongated shape. Figure 9-b pass 3 annealed condition. It can be seen that annealing has had little effect on the microstructure.

(a)

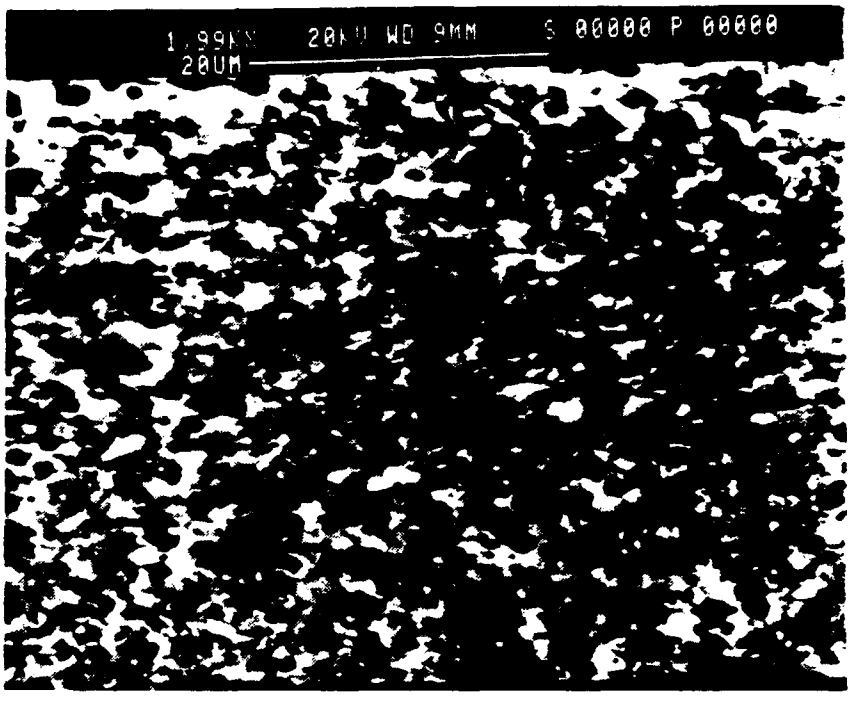

(b)

Figure 8. Backscattered SEM Micrograph Showing the Al-10Mg Alloy Following Rolling Pass 12: a.) In the As-rolled Condition, b.) Following 25 Minutes of Annealing at 300°C.

(a)

(b)

Figure 9. Backscattered SEM Micrograph Showing the Al-10Mg-0.2Mn Alloy Following Rolling Pass 3: a.) In the As-rolled Condition, b.) Following 25 Minutes Of Annealing at 300°C.

The as-rolled microstructure following pass 8, presented in Figure 10-a, shows increased precipitation when compared with pass 3. The light contrast around prior grain boundaries suggest the occurrence of recrystallization along these boundaries. Also, there is some localized contrast in the vicinity of some precipitates. Upon annealing (Figure 10-b), there is no apparent increase in particle size. However there are isolated instances of recrystallization at some larger particles and in the vicinity of clusters of smaller particles. Comparing Figures 10-b and 9-b shows that the amount of $MnAl_6$ has remained virtually unchanged from previous passes, and that many of these particles have retained their elongated shape.

Figure 11-a shows microstructure in the as-rolled condition following pass 12. Comparison with pass 8 (Figure 10-a) shows an increasingly uniform distribution of β precipitates. The mottled, featureless appearance of the matrix possibly indicates extensive deformation in previously recrystallized grains. After annealing, the fully processed material of Figure 11-b shows large areas of recrystallization; although some regions of recovery can still be seen. Additionally, some particles show evidence of newly nucleating grains.

(a)

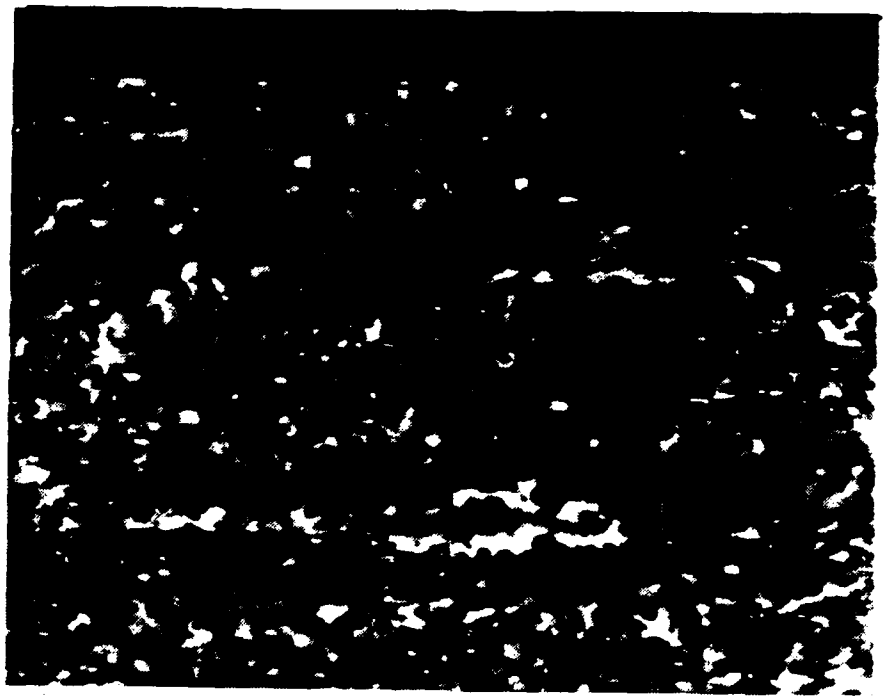

(b)

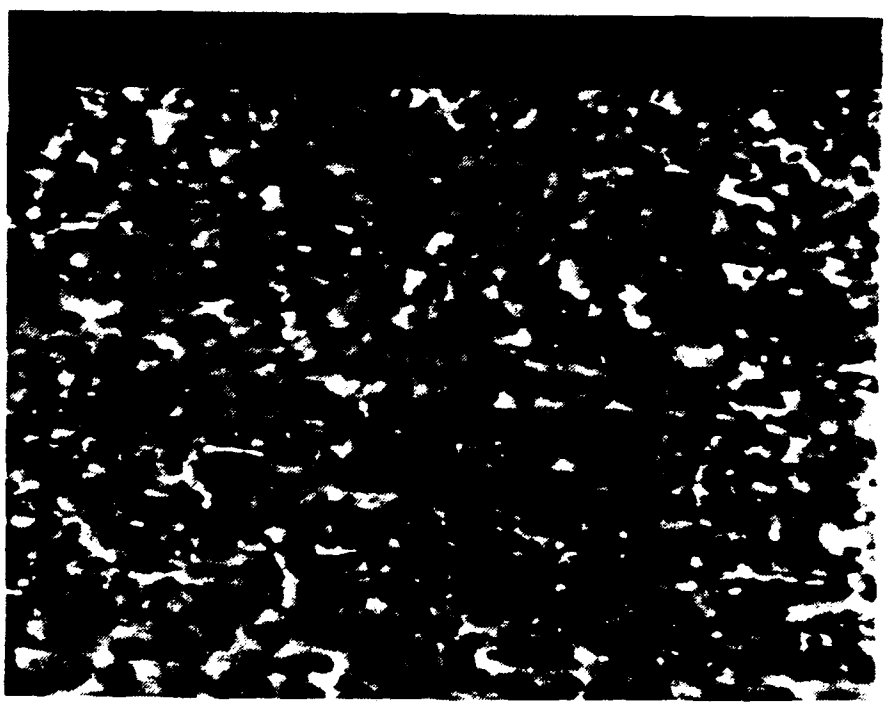

Figure 10. Backscattered SEM Micrograph Showing the Al-10Mg-0.2Mn Alloy Following Rolling Pass 8: a.) In the Annealed Condition, b.) Following 25 Minutes of Annealing at 300°C.

(a)

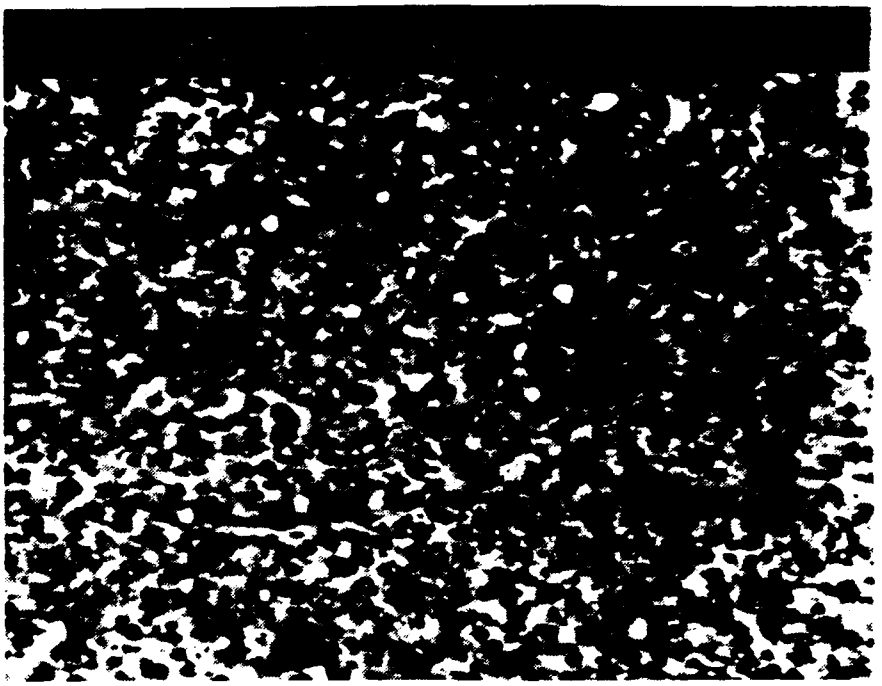

(b)

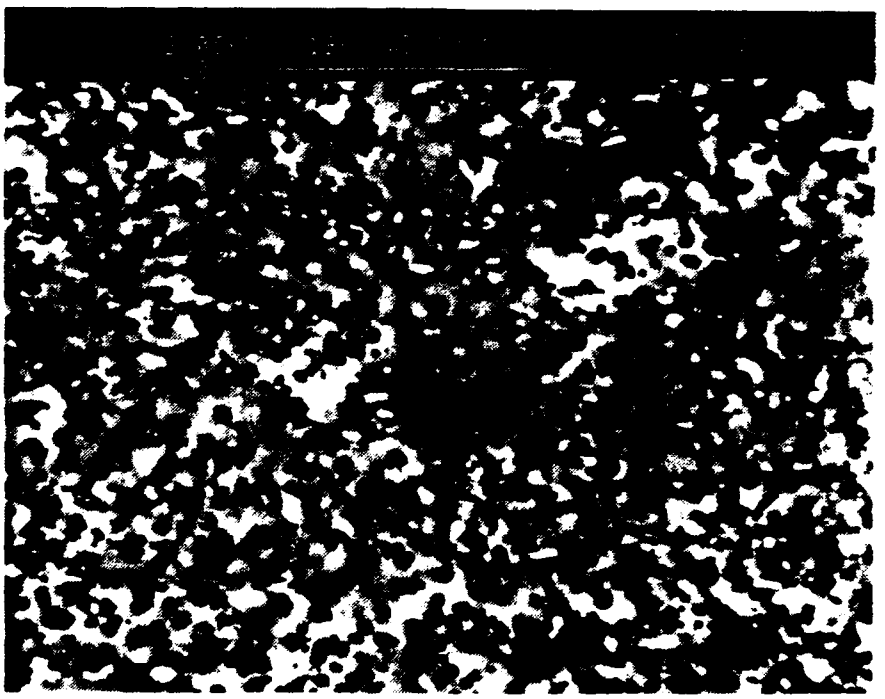

Figure 11. Backscattered SEM Micrograph Showing the Al-10Mg-0.2Mn Alloy Following Rolling Pass 12: a.) In the As-rolled Condition, b.) Following 25 Minutes of Annealing at 300°C.

3. Al-10Mg-0.5Mn

The as-rolled microstructure following pass 3 is shown in Figure 12-a. The β precipitate volume fraction is relatively higher when compared with either the Al-10Mg or the Al-10Mg-0.2Mn alloys. This suggests an increase in precipitation with increasing Manganese content. Also, more $MnAl_6$ particles are seen at this stage than previously. Examination of the precipitates reveals many β particles have again heterogeneously nucleated on $MnAl_6$ particles. There is also continued β-phase precipitation on prior grain boundaries and within the matrix. As before, many of the $MnAl_6$ particles are elongated. Figure 12-b, representing the annealed pass 3 microstructure, reveals that there is little change in the microstructure upon annealing.

Further in the rolling process, following pass 8, the as-rolled microstructure shows increased β-phase precipitation (Figure 13-a). Comparison with Figure 12-a shows that the β particles are more uniformly dispersed than following pass 3, and that some have coarsened. Many of the $MnAl_6$ particles have retained their elongated shape, and are now generally aligned with the rolling direction. Evidence of local lattice rotation can be seen adjacent to some larger particles, but the matrix material appears predominately recovered. Figure 13-b shows the effect of annealing. Additional β-phase coarsening appears to have occurred. There is now evidence of some isolated recrystallization around the largest particles and in

(a)

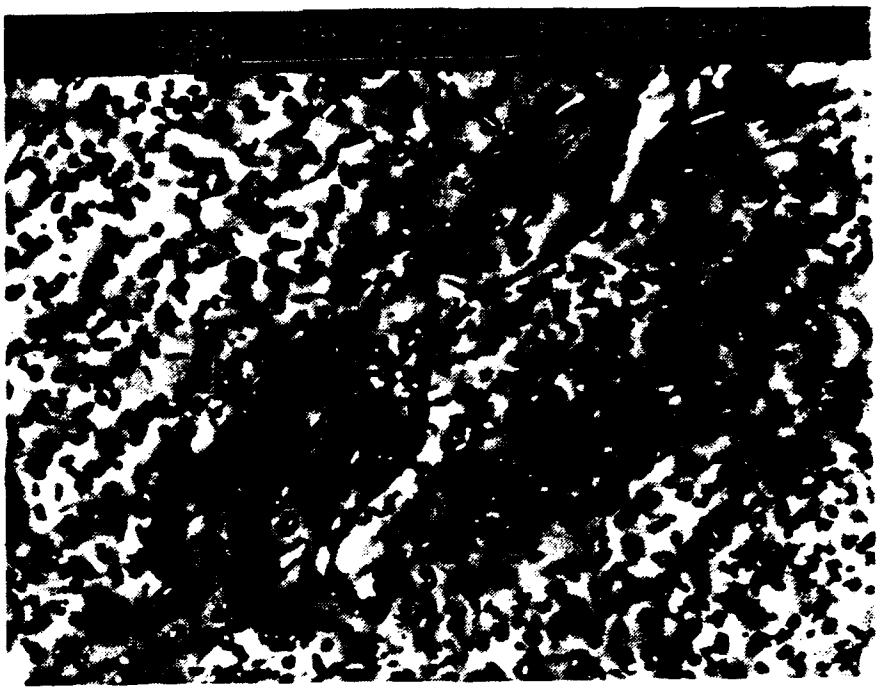

(b)

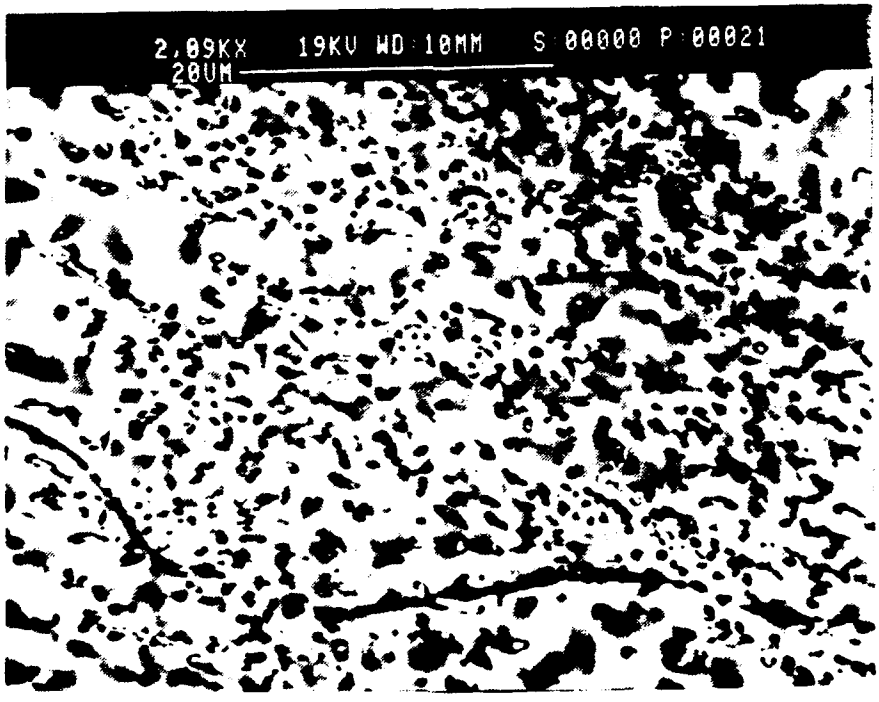

Figure 12. Backscattered SEM Micrograph Showing the Al-10Mg-0.5Mn Alloy Following Rolling Pass 3: a.) In the As-rolled Condition, b.) Following 25 Minutes of Annealing at 300°C.

(a)

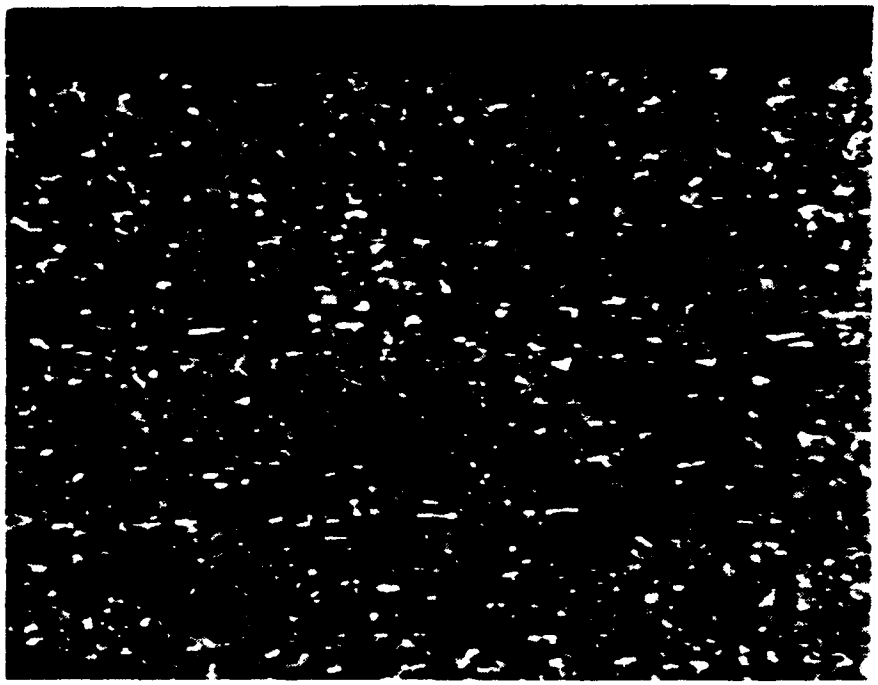

(b)

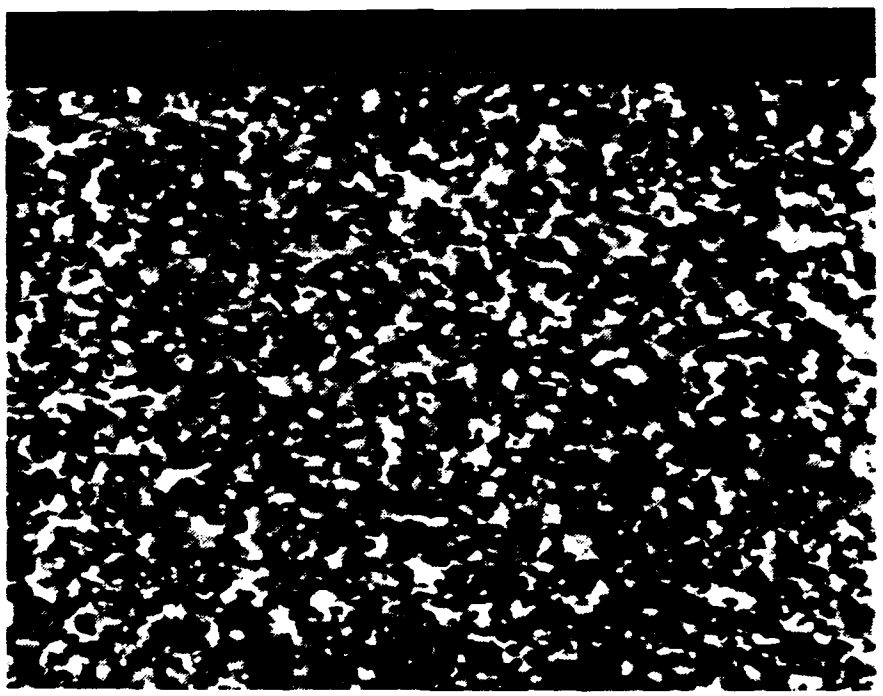

Figure 13. Backscattered SEM Micrograph Showing the Al-10Mg-0.5Mn Alloy Following Rolling Pass 8: a.) In the As-rolled Condition, b.) Following 25 Minutes of Annealing at 300°C.

association with clusters of smaller particles. In general, however, the matrix remains mostly recovered.

The as-rolled microstructure following pass 12 is presented in Figure 14-a. Some β-phase particle coarsening can be seen. Newly recrystallized grains are apparent in the matrix as well as deformed prior recrystallized grains. Many of the elongated $MnAl_6$ particles of Figure 13-a now seem to have broken up. Figure 14-b reveals that upon annealing there is no apparent particle coarsening and no apparent increase in recrystallization. At this final stage of processing the material continues to exhibit regions of recovery.

B. MECHANICAL TESTING RESULTS

The microstructure following pass 12 and subsequent annealing represents the material in the fully processed condition. This condition is similar to the condition of the material at the start of mechanical testing. Constant crosshead-speed tensile tests to failure were conducted at 300°C on each alloy. From these tests ductility, stress-strain, and strain rate sensitivity information were determined. These results combine to determine the superplastic response of the materials during straining.

1. Stress-Strain Characteristics

True stress-true plastic strain curves for each alloy are shown in Figures 15-17. Curves representing seven different strain rates are plotted in each case. Examination

(a)

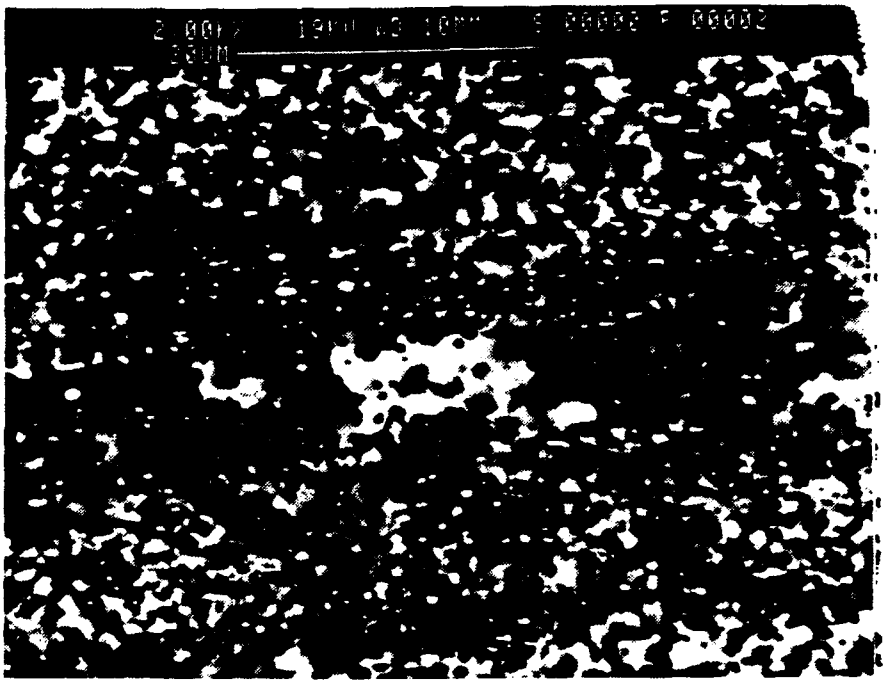

(b)

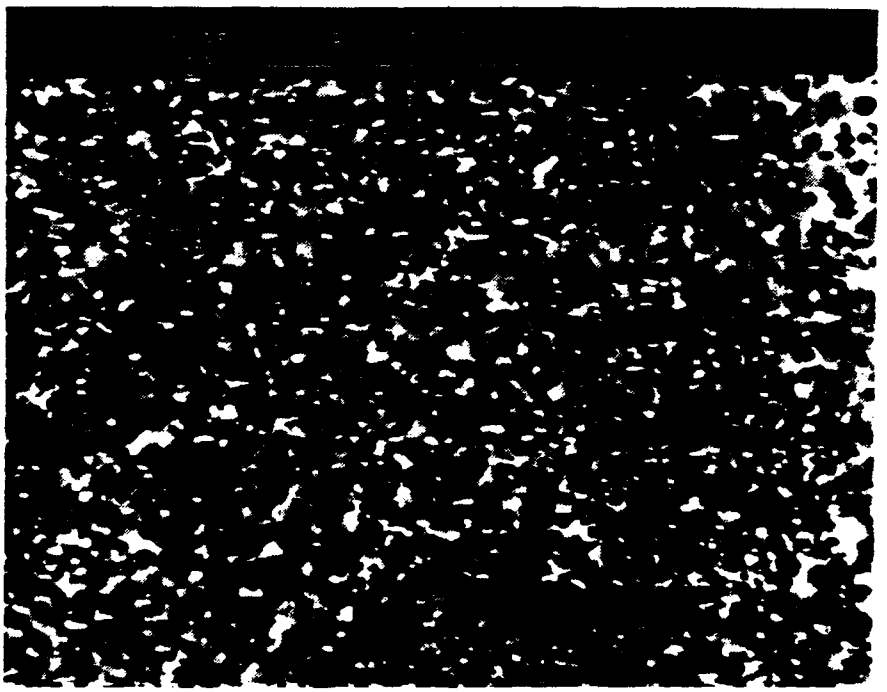

Figure 14. Backscattered SEM Micrograph Showing the Al-10Mg-0.5Mn Alloy Following Rolling Pass 12: a.) In the As-rolled Condition, b.) Following 25 Minutes of Annealing at 300°C.

of the curves shows that at no time during straining do any of the materials exhibit steady-state behavior. Substantial strain hardening occurs at the initial stages of deformation, as stress values initially increase. Comparison of Figures 15, 16, and 17 reveals that the maximum stress achieved at each strain rate decreases with increasing Mn content, indicating that the addition of Mn weakens the material. The observed softening behavior may reflect several factors. Firstly the assumptions of constant volume and uniform cross sectional area upon which the true stress versus true plastic strain data were calculated, may not be valid. In this case diffuse necking of the sample, or cavitation within the sample during straining, may affect the flow stress values. Previous work has, however, suggested that cavitation is unlikely at strain values below 1.0 [Ref. 8]. Microstructural instability in the form of grain size changes during straining may also affect the flow stresses as related by Equation (3).

In the region immediately following the maximum stress values the curves are concave upwards. This concavity becomes increasingly evident with decreasing strain rate and increasing Mn content. The concave upwards region of the curves is followed by region of localized necking, which is indicated by a concave down region of the curve. This behavior is especially evident at lower strain rates where the duration of localized necking is longest. The localized necking is followed by failure.

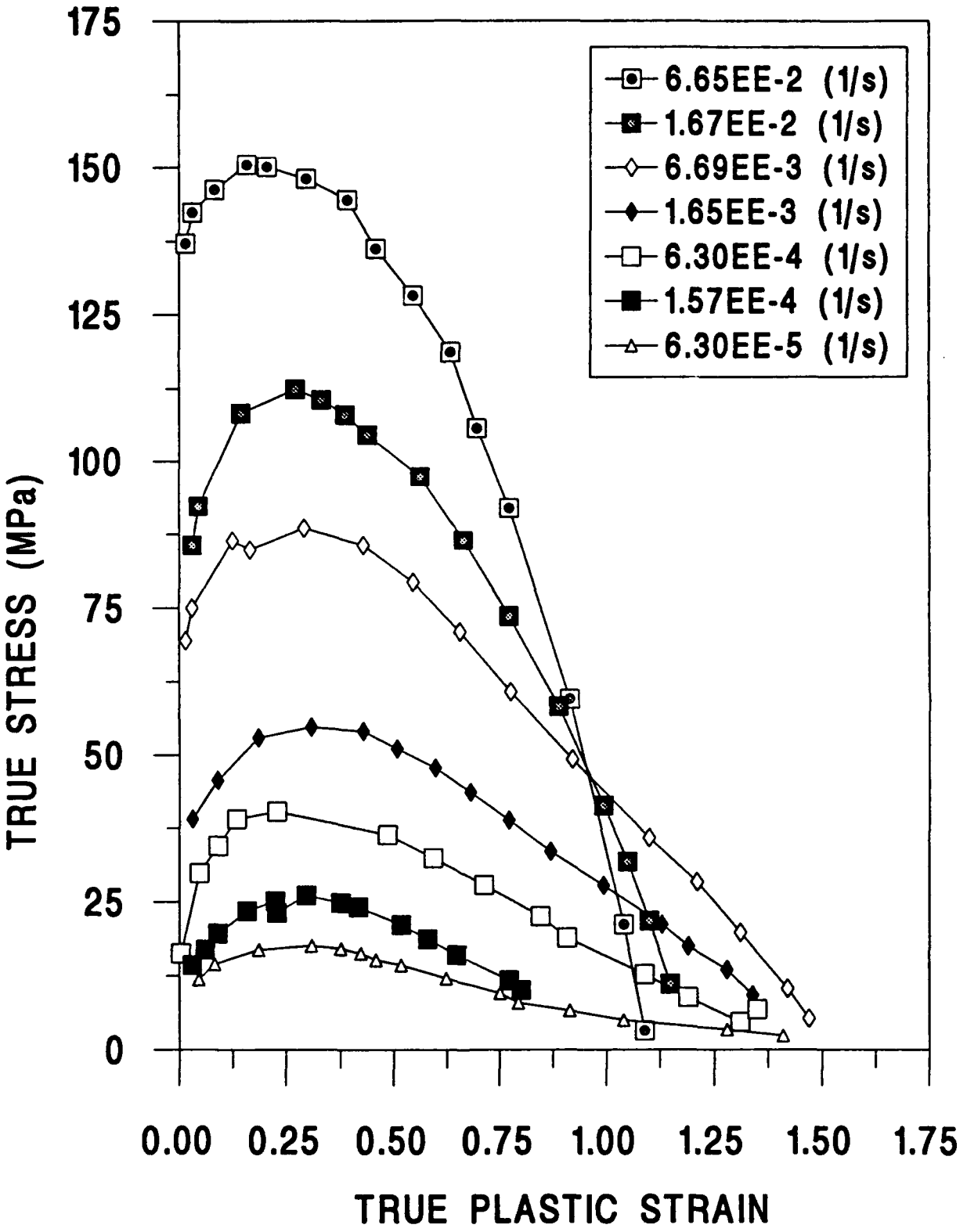

Figure 15. True Stress vs True Plastic Strain Curves for the Al-10Mg Alloy at 300°C for Seven Different Strain Rates.

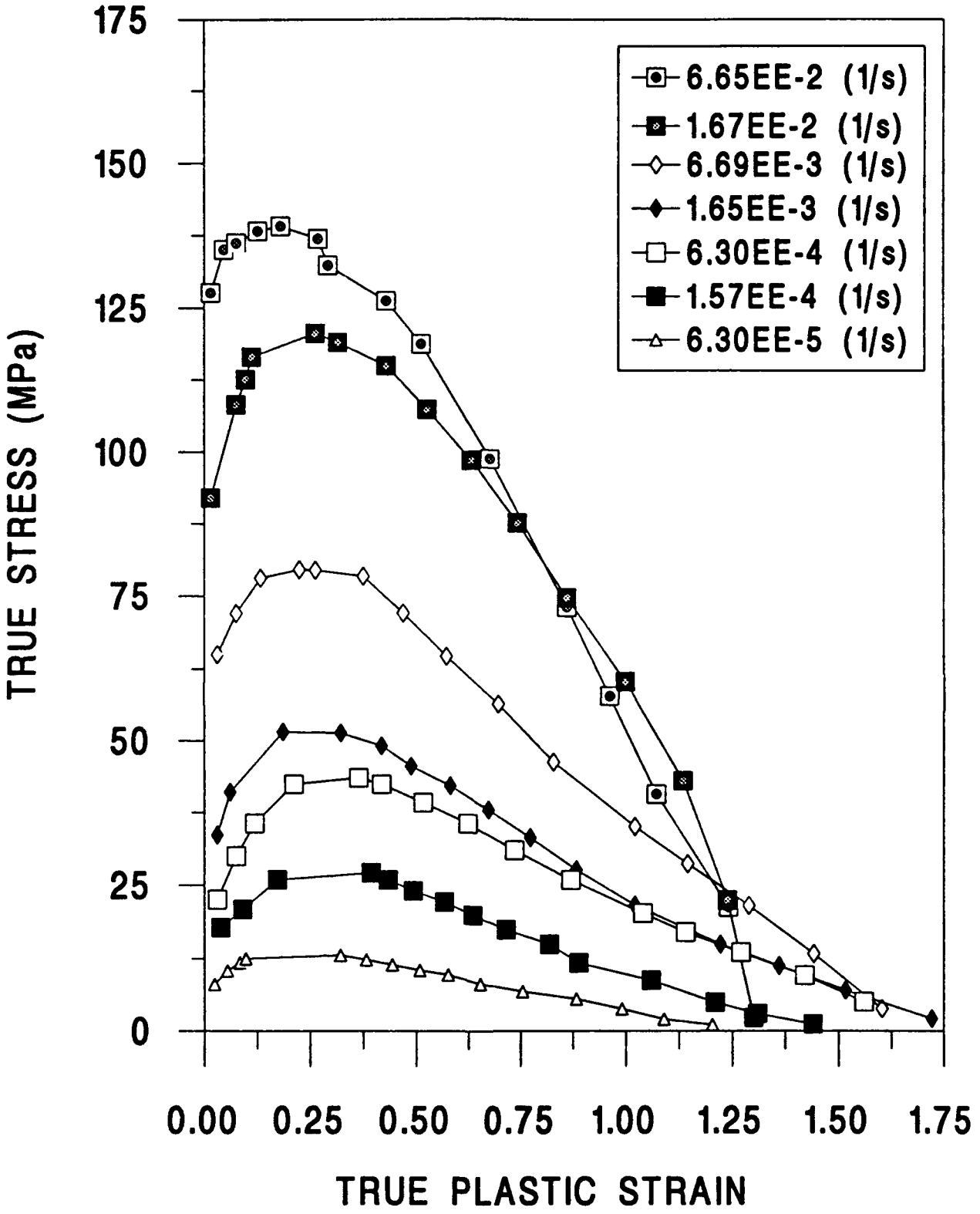

Figure 16. True Stress vs True Plastic Strain Curves for the Al-10Mg-0.2Mn Alloy at 300°C for Seven Different Strain Rates.

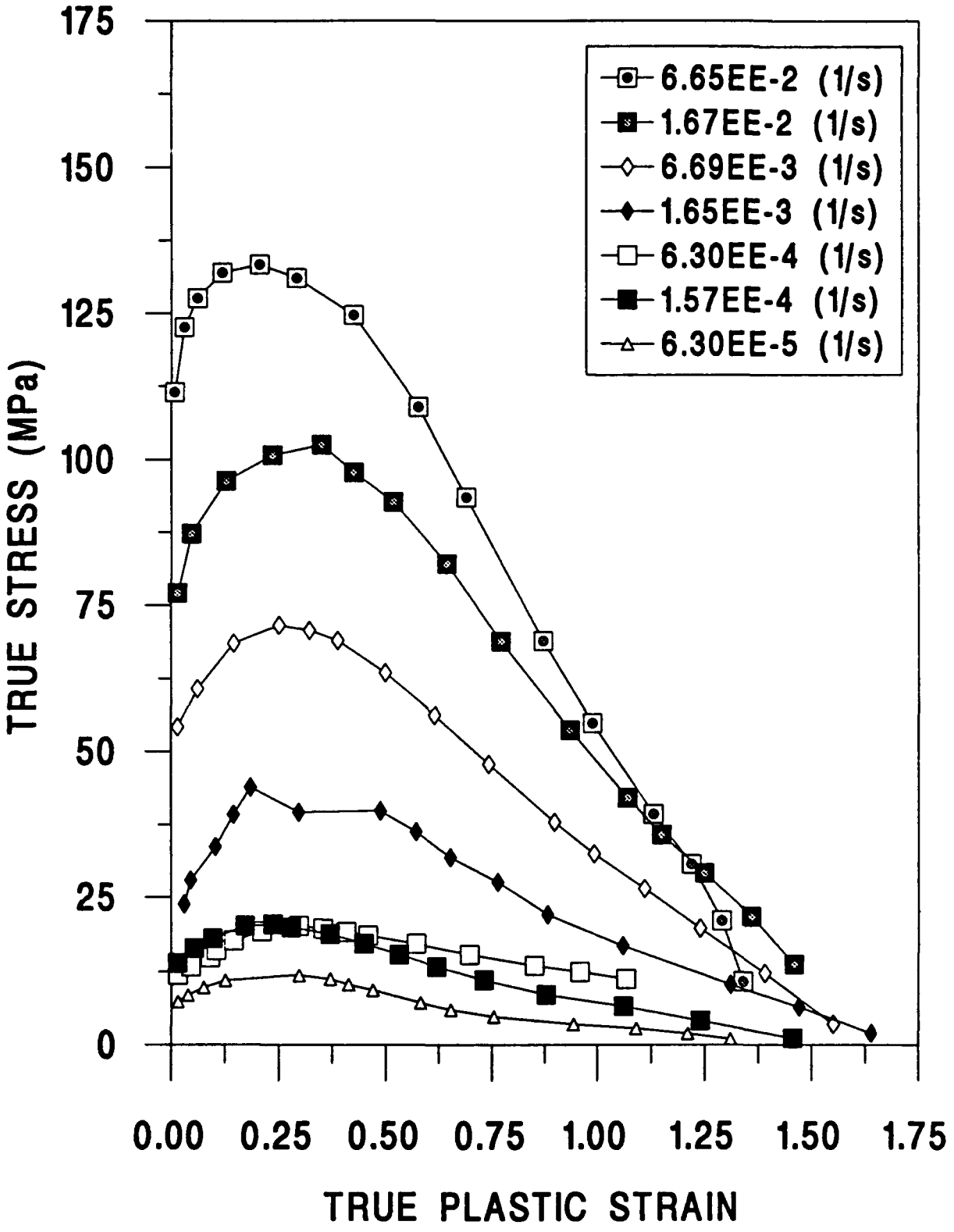

Figure 17. True Stress vs True Plastic Strain Curves for the Al-10Mg-0.5Mn Alloy at 300°C for Seven Different Strain Rates.

2. Stress-strain Rate Characteristics

Resistance to localized necking is a characteristic of superplastic flow. A material with a high strain rate sensitivity coefficient, m, resists localized necking and consequently is more ductile. The coefficient, m, is given by

$$m=\left.\frac{\partial \ln \sigma}{\partial \ln \dot{\varepsilon}}\right|_{\varepsilon} \qquad (6)$$

where σ is the true stress and $\dot{\varepsilon}$ is the strain rate. Thus, m can be determined as the slope of a stress versus strain rate plot on double logarithmic axes. Figures 18-20 show the stress versus strain rate plots for each alloy at true strains of ε = 0.02 to ε = 0.3. It can be seen that in general the slopes of these lines are greater for lower strains. Also, the slopes increase with increasing Mn content. Thus it can be concluded that the strain rate sensitivity coefficient decreases with increasing strain, and increases with increasing Mn content.

At strains beyond the maximum flow stress, diffuse necking of the samples becomes a possibility. For this reason the stress versus strain rate curves for strains above ε = 0.3 are plotted on separate graphs. See Figures 21, 22, and 23. Figure 24 and Table VIII summarize m values for each alloy as a function of strain. The initial high m values at low strains are clearly evident. These m values indicate a contribution to deformation by grain boundary sliding in all of these materials. There is then a gradual decrease in the m-values as

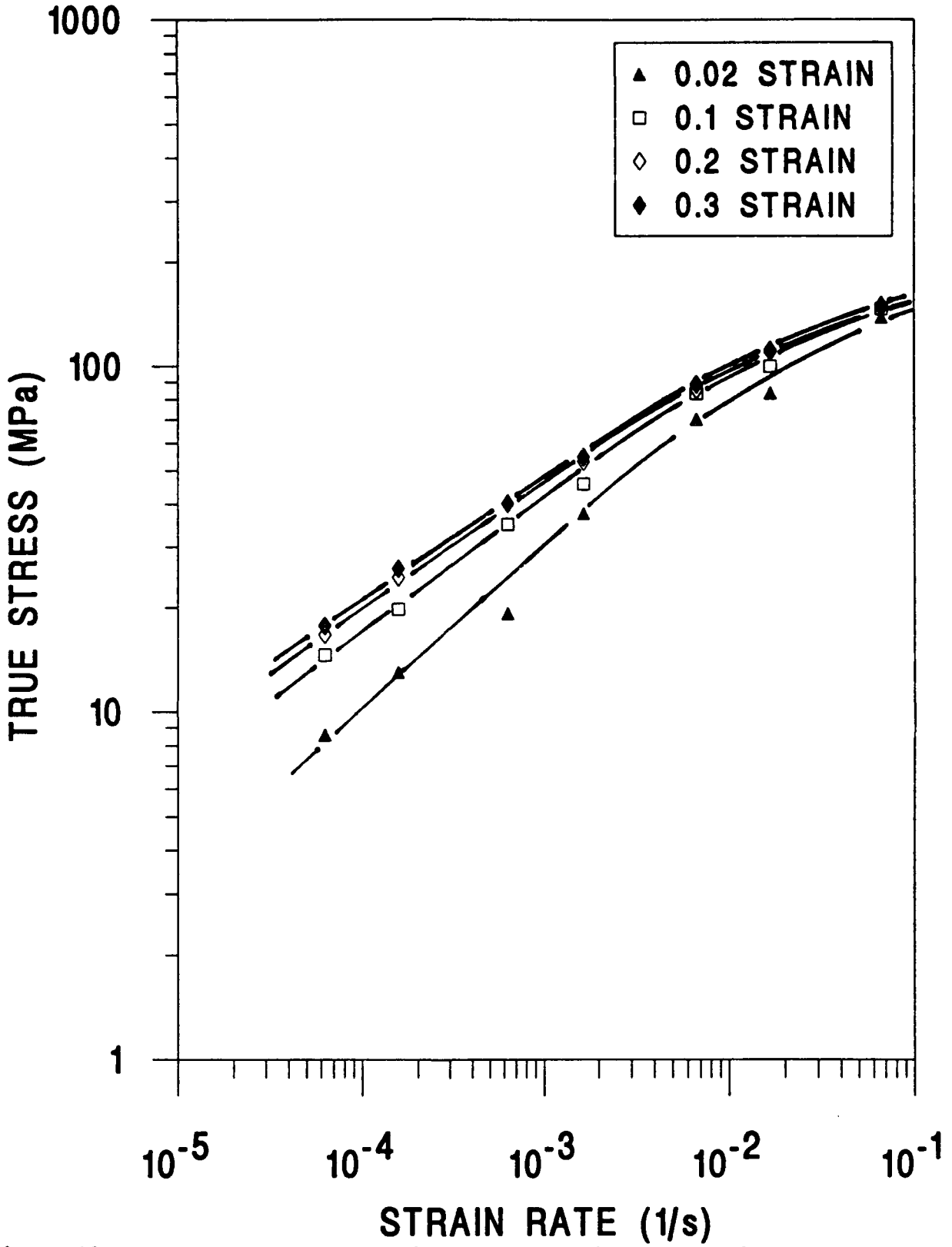

Figure 18. True Stress vs Strain Rate Curves for the Al-10Mg Alloy at 300°C for True Strains Between 0.02 and 0.3.

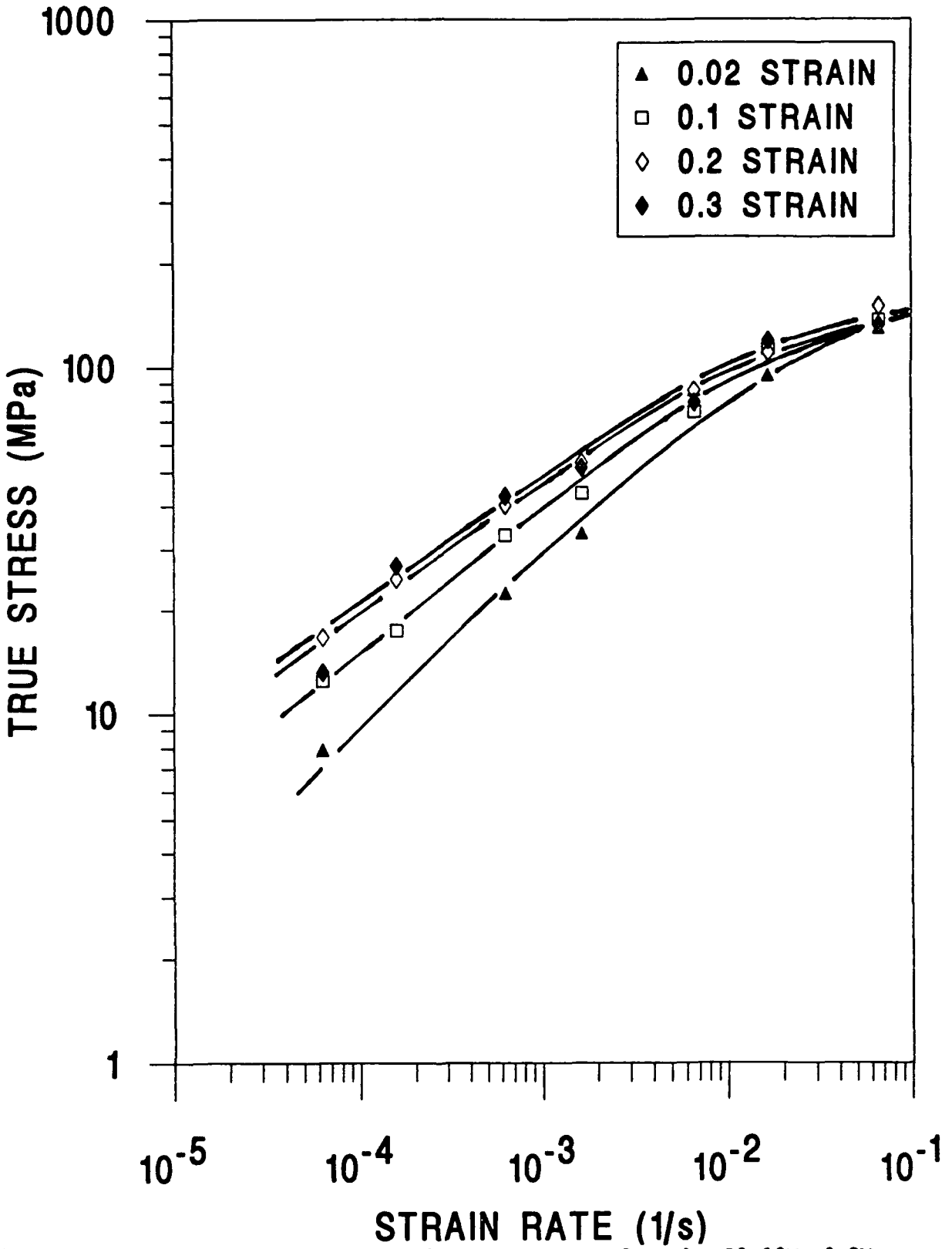

Figure 19. True Stress vs Strain Rate Curves for the Al-10Mg-0.2Mn Alloy at 300°C for True Strains Between 0.02 and 0.3.

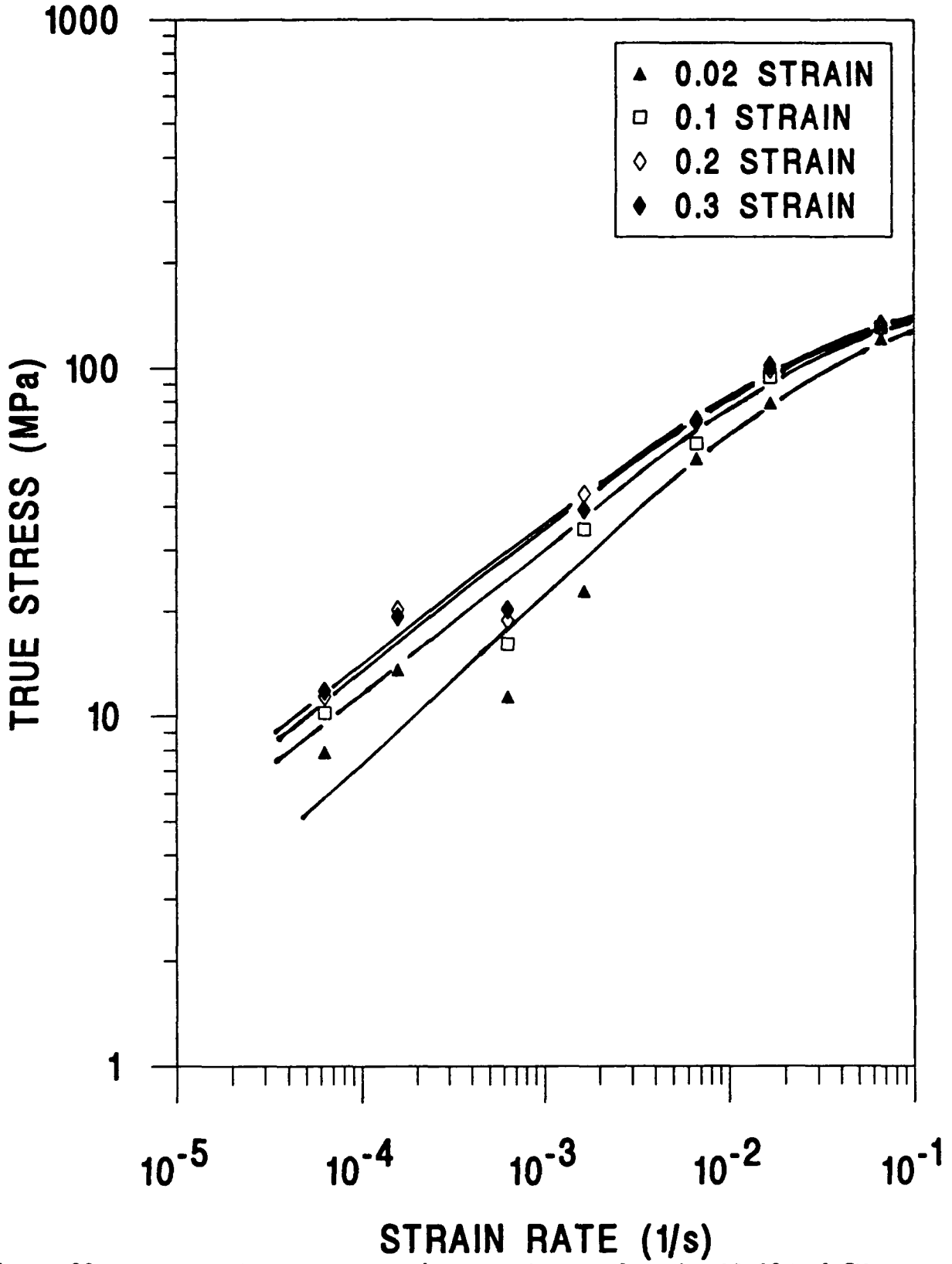

Figure 20. True Stress vs Strain Rate Curves for the Al-10Mg-0.5Mn Alloy at 300°C for True Strains Between 0.02 and 0.3.

the strain increases. The binary alloy tends to a value of m ≈ 0.33. This behavior is consistent with a transition in deformation mechanisms to one of dislocation glide control of deformation [Ref. 3]. The fact that m tends to larger values for the Mn containing materials suggests a finer initial microstructure, and that such a transition is incomplete. The overall tendency of the strain rate sensitivity coefficients to decrease reflects grain growth during deformation, as explained by Equation (3). However, with further straining the m-values unexpectedly rise. This effect is opposite to that expected if grain growth continues to occur. However, the observed increase may reflect one or more of the mechanisms suggested earlier for flow softening. Diffuse necking may occur in such a way as to produce anomolously low stress values. Also, at lower strain rates, cavitation may affect m values. It is also possible that the explanation for this phenomenon may be similar to that given for similar behavior in SUPRAL alloys. In these materials, initial low m-values increase with straining as the microstructure refines through continuous recrystallization [Ref. 14]. In the materials considered here, a similar effect, particle stimulated nucleation of recrystallization, may begin to occur at strains of $\dot{\epsilon} \approx 0.30$. If so, microstructural refinement due to the formation of new, recrystallized grains may account for the increase in m. Distinguishing among these possibilities

would require detailed microscopy of material deformed to strains less than the failure strain prior to examination.

TABLE VIII. STRAIN RATE SENSITIVITY COEFFICIENTS, m

TRUE STRAIN	Al-10Mg	Al-10Mg	Al-10Mg
0.02	0.394	0.439	0.429
0.10	0.358	0.382	0.390
0.20	0.329	0.366	0.378
0.30	0.329	0.359	0.381
0.50	0.371	0.378	0.409
1.00	0.448	0.464	0.457

3. Ductility

Figures 25, 26, and 27 summarize the ductility data for each alloy. The generally lower ductilities for the binary alloy reflect the lower associated m values. Ductilities for the Al-10Mg-0.2Mn alloy are uniformly higher than those of the binary alloy, reflecting its m values. However there is no subsequent further increase in ductility for higher m values. However there is no subsequent further increase in ductility for the Al-10Mg-0.5Mn alloy compared to the Al-10Mg-0.2Mn alloy, as the m values would suggest. It is however evident that the Al-10Mg-0.5Mn material is more ductile than the binary alloy, especially at the higher strain rates.

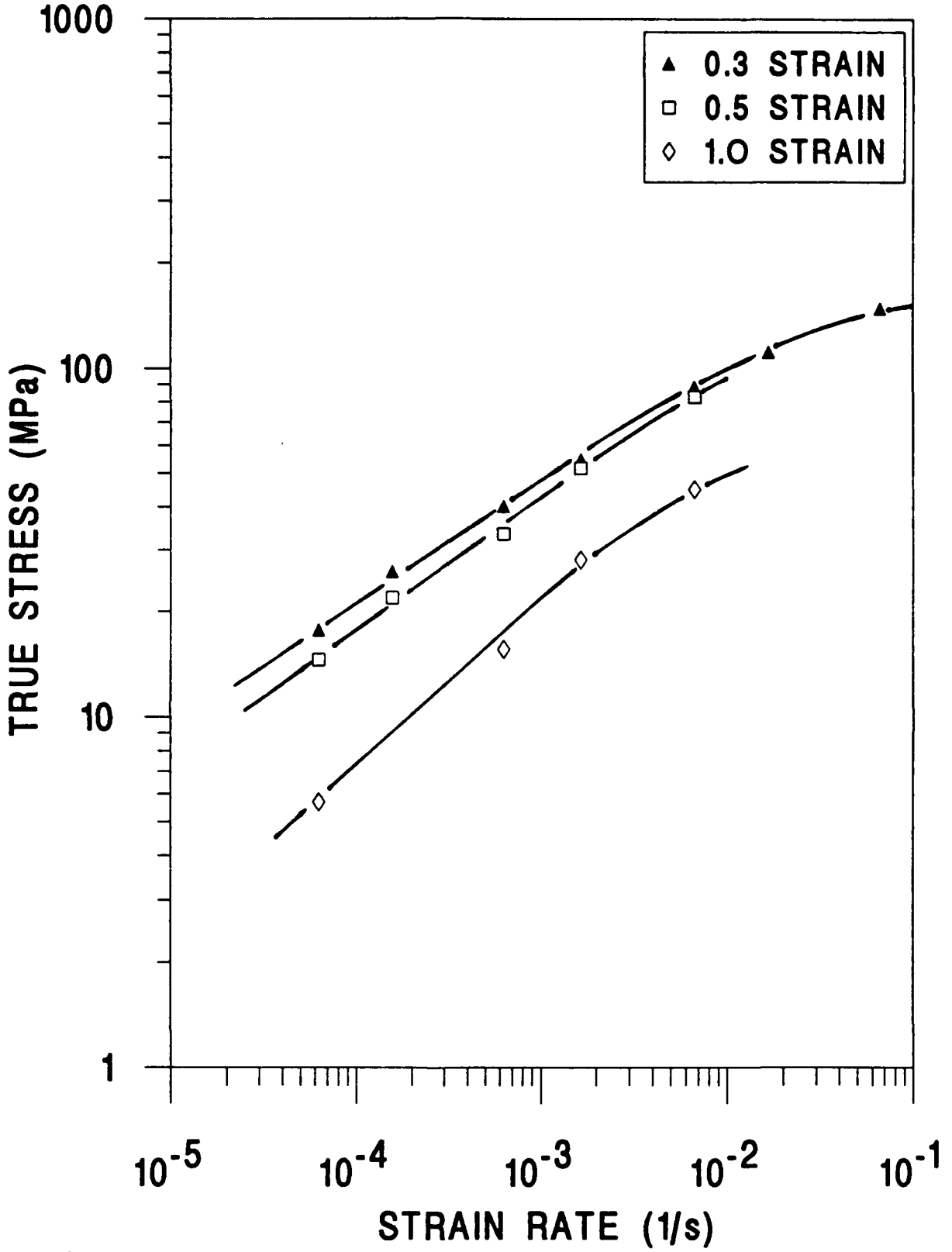

Figure 21. True Stress vs Strain Rate Curves for the Al-10Mg Alloy at 300°C for True Strains Greater than 0.3.

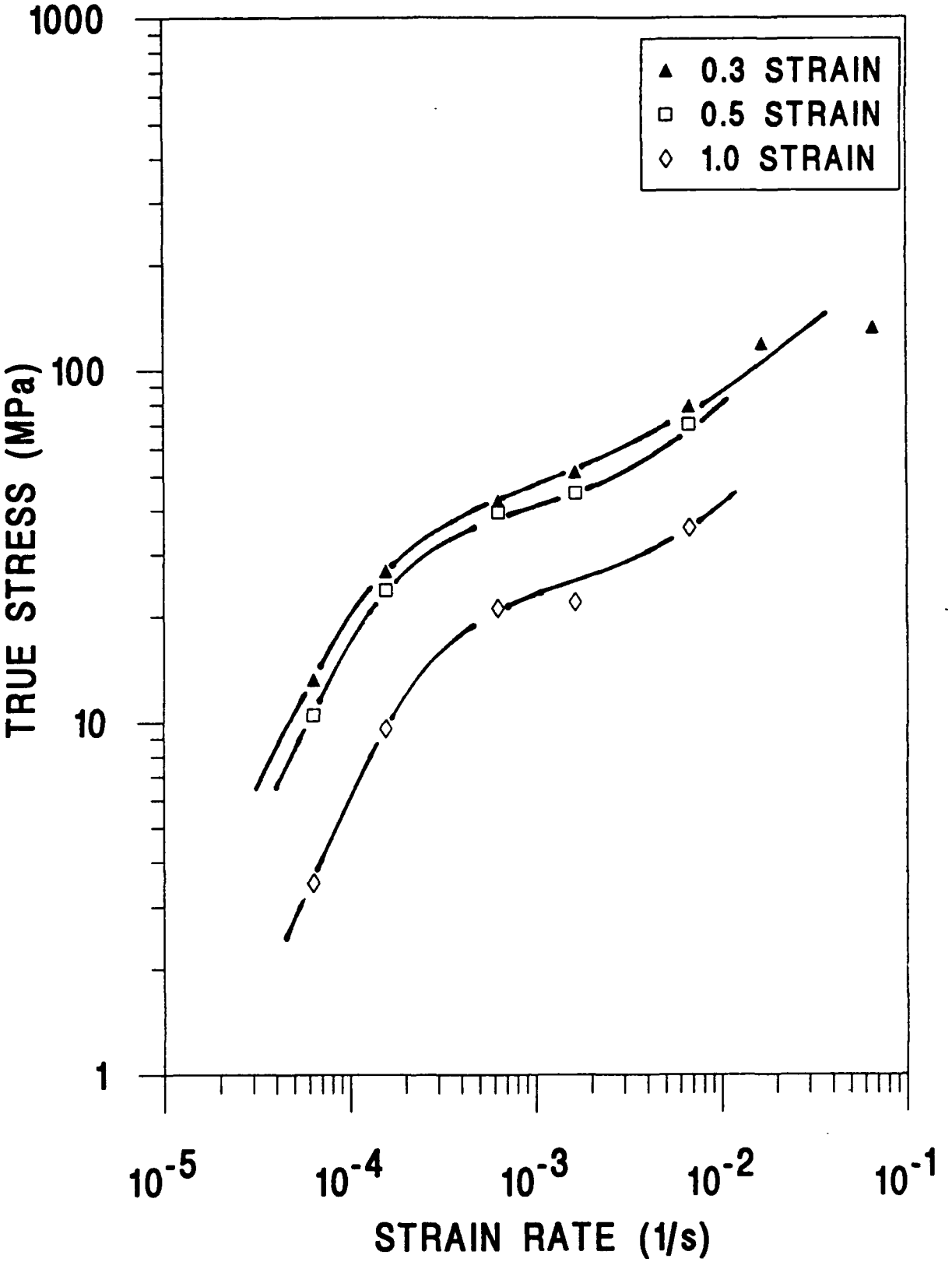

Figure 22. True Stress vs Strain Rate Curves for the Al-10Mg-0.2Mn Alloy at 300°C for True Strains Greater than 0.3.

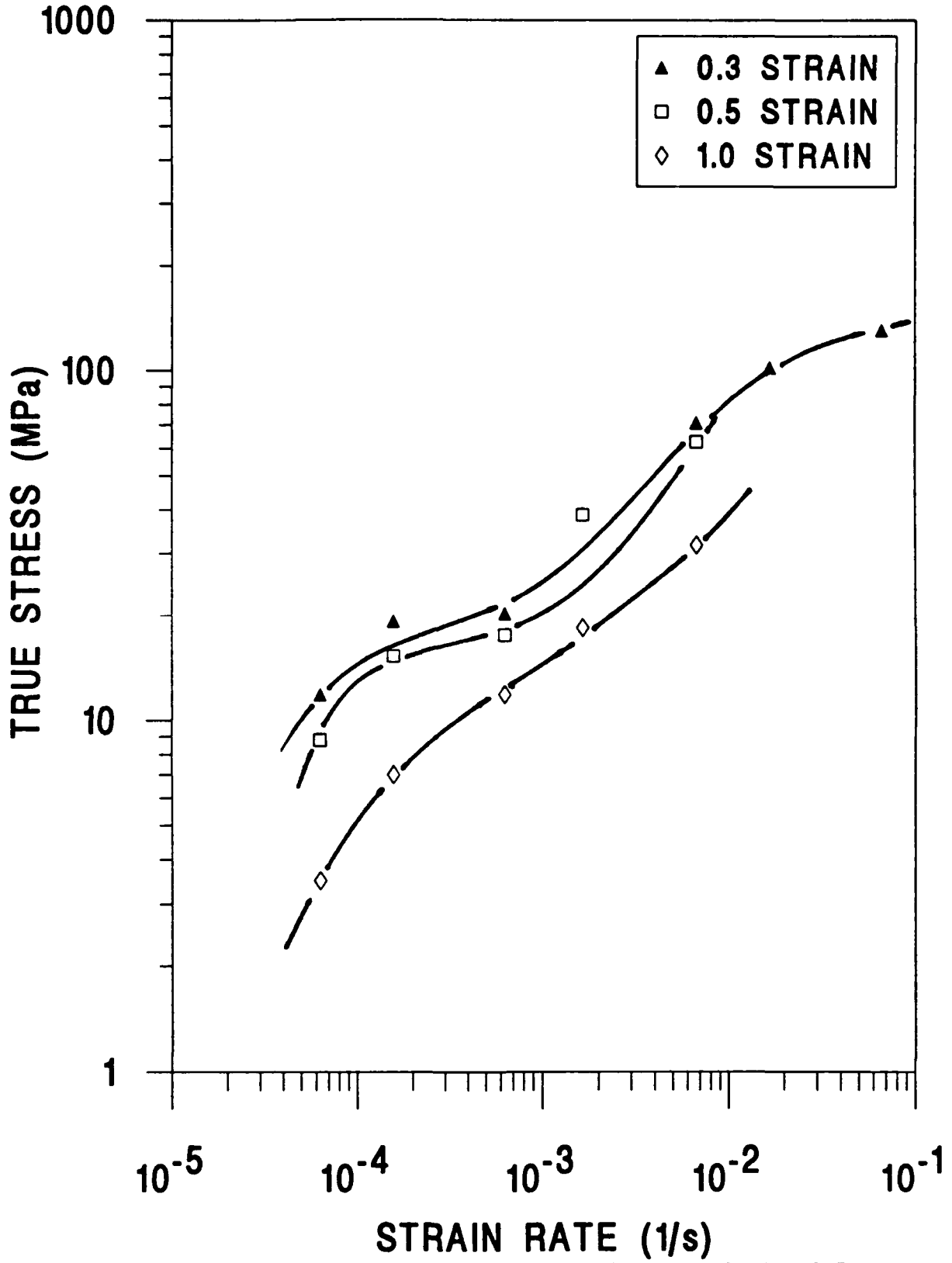

Figure 23. True Stress vs Strain Rate Curves for the Al-10Mg-0.5Mn Alloy at 300°C for True Strains Greater than 0.3.

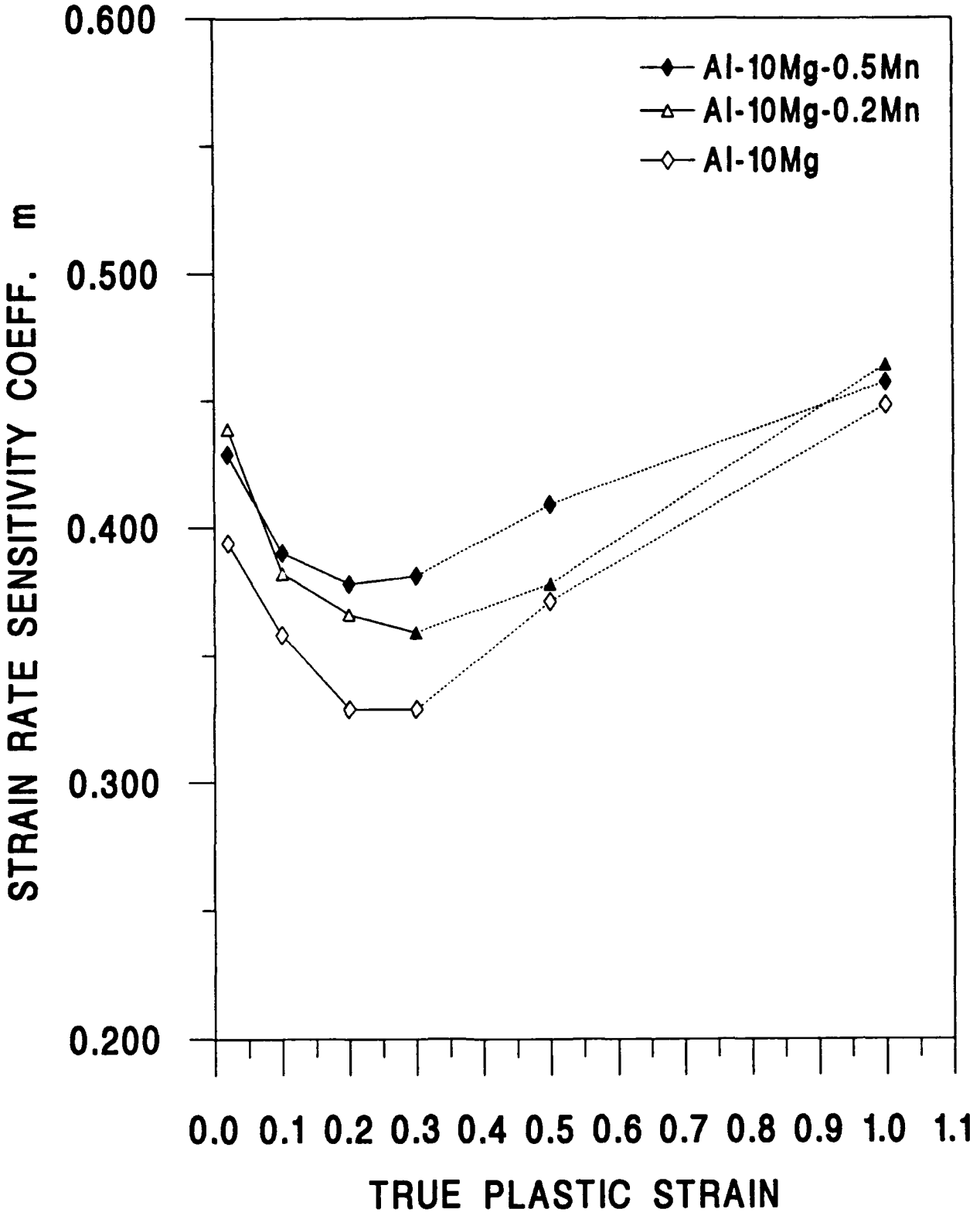

Figure 24. Plot of Strain Rate Sensitivity Coefficients vs True Plastic Strain at 300°C for the Three Alloys Considered.

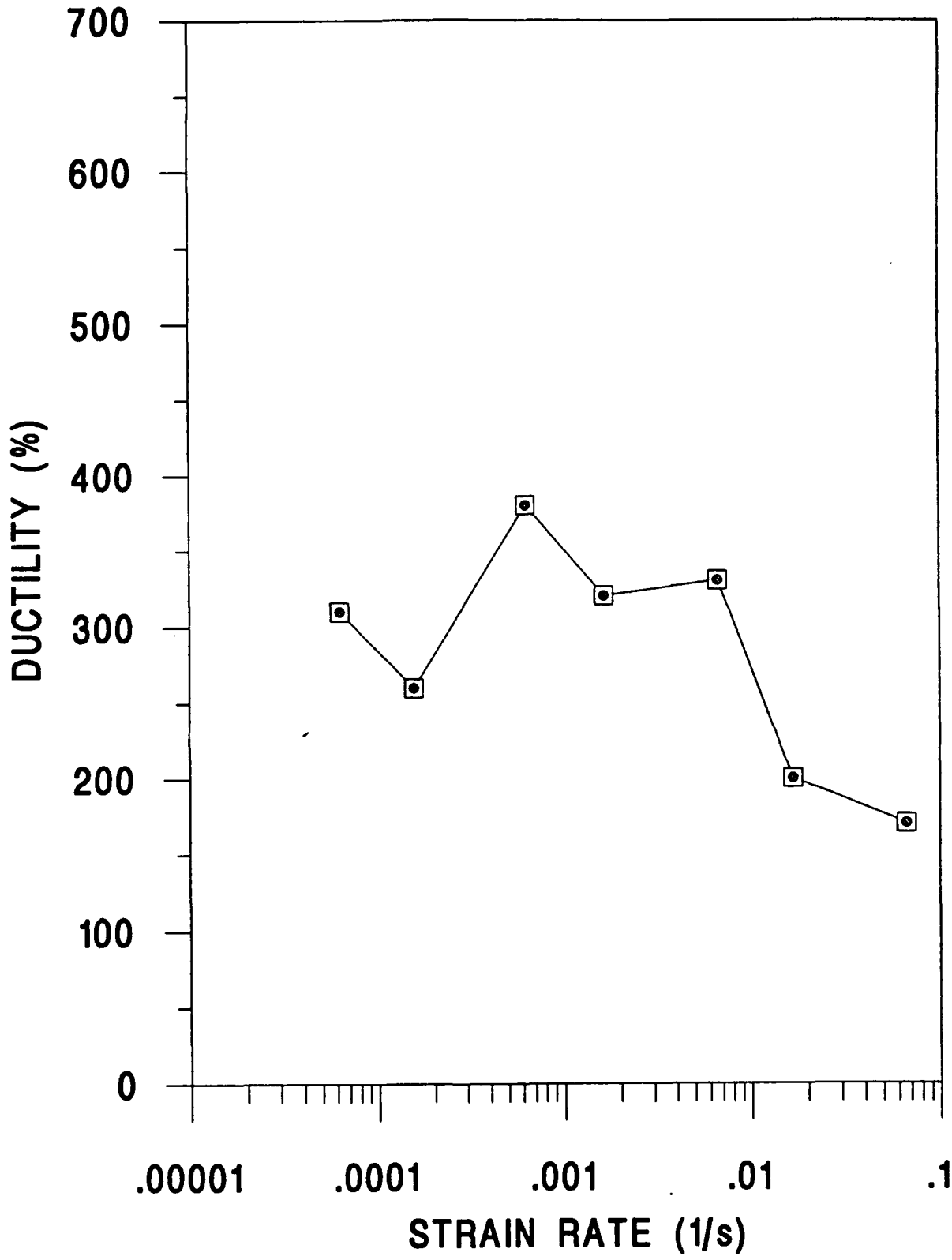

Figure 25. **Ductility vs Strain Rate at 300°C for the Al-10Mg Alloy.**

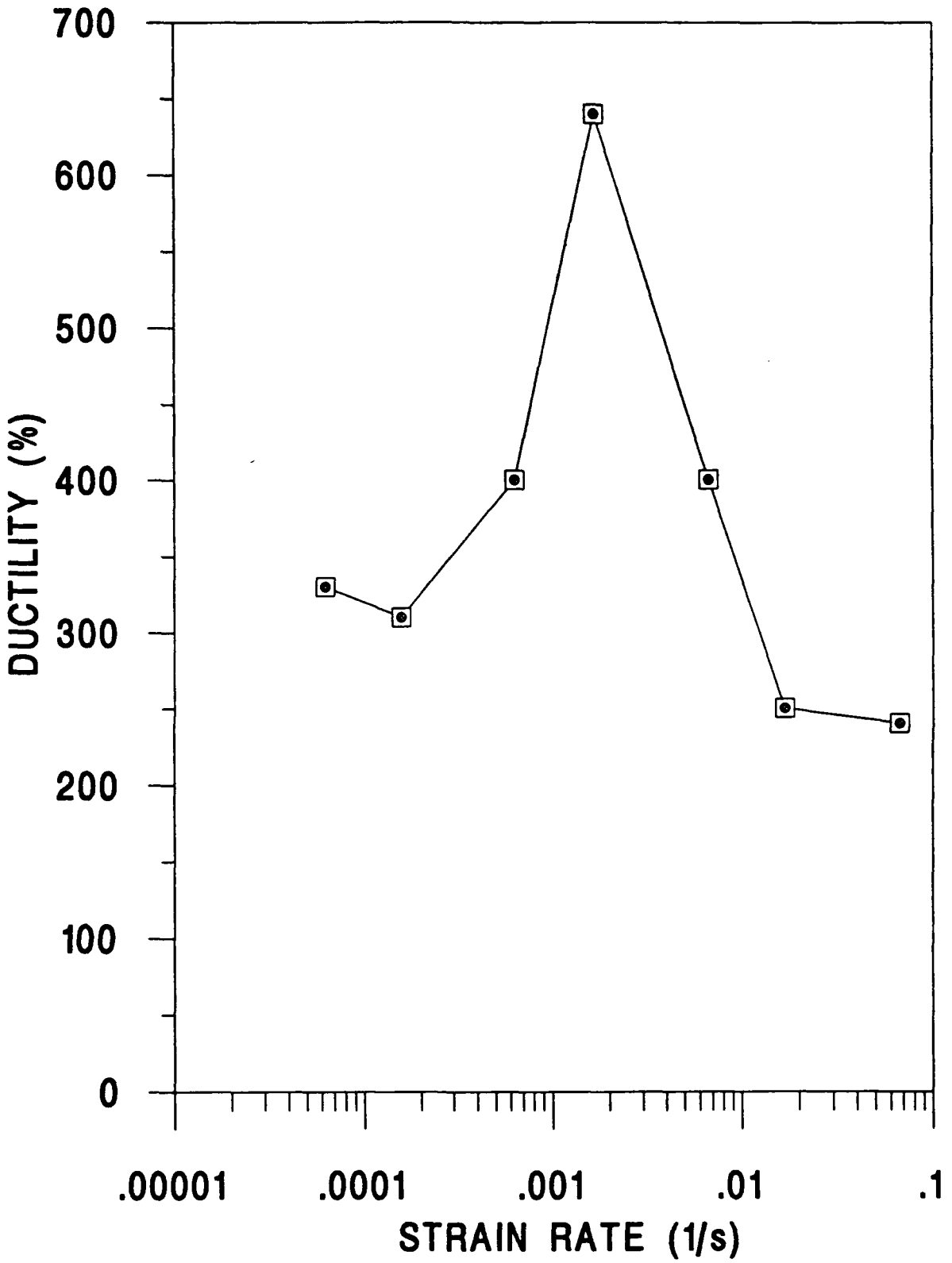

Figure 26. Ductility vs Strain Rate for the Al-10Mg-0.2Mn Alloy at 300°C.

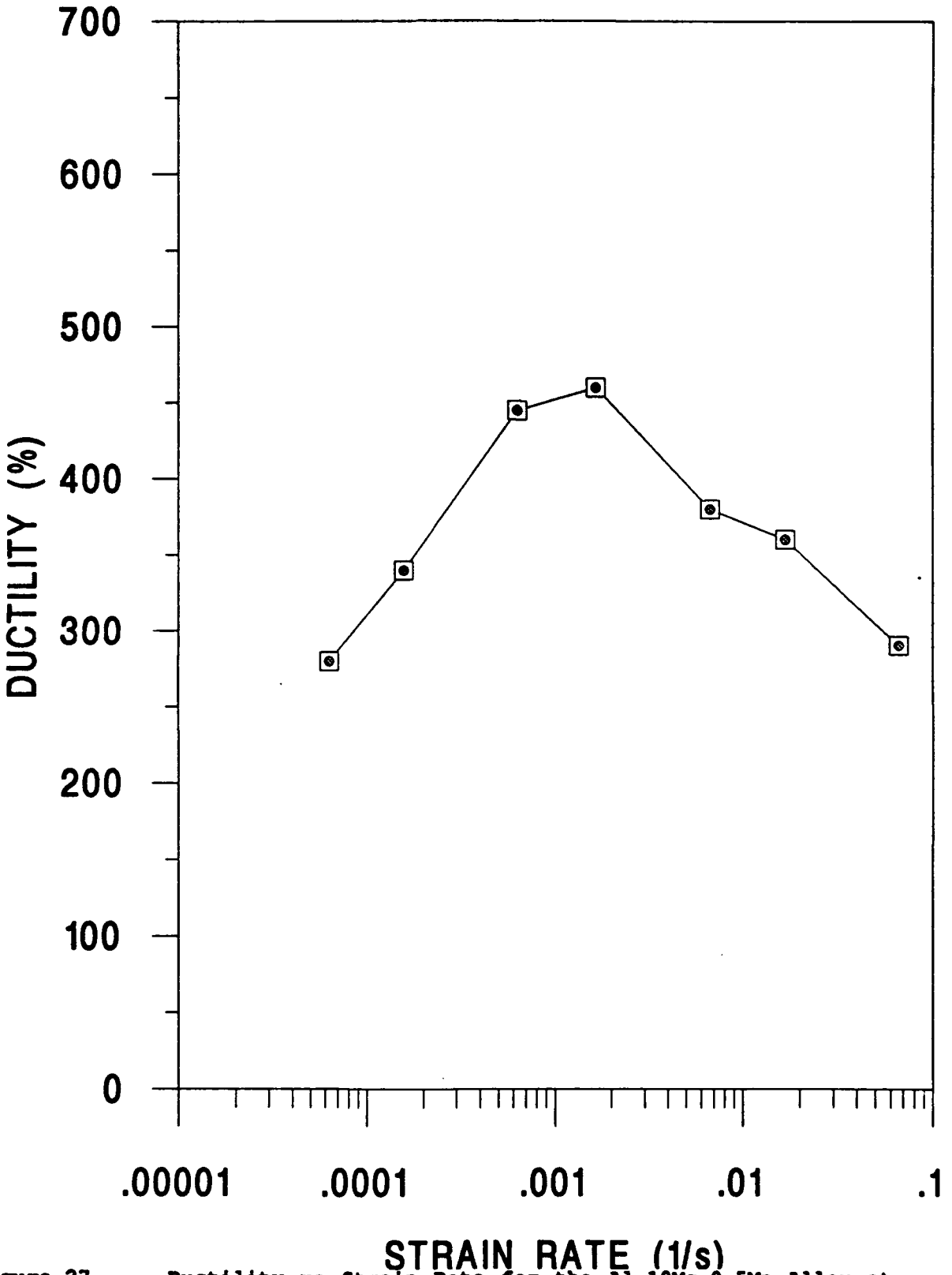

Figure 27. Ductility vs Strain Rate for the Al-10Mg-0.5Mn Alloy at 300°C.

The addition of Mn does then increase the superplastic response of the Al-Mg system. The fact that the Al-10Mg-0.5Mn alloy is not more superplastic may be a reflection of microstructural considerations. The high $MnAl_6$ particle content of the fully processed Al-10Mg-0.5Mn alloy may inhibit grain boundary sliding, accounting for the lower ductility. Such a result would suggest an upper limit of Mn which is beneficial to superplastic deformation. Also, cavitation at $MnAl_6$ particles may occur. A detailed microstructural analysis of volume fraction of precipitates and particle size as they evolve during straining would be needed to answer this question.

C. DISCUSSION

These results show that the as processed materials are superplastic. Microstructural evidence shows that, in the early stages of the TMP, precipitation reactions dominate. In the binary alloy this precipitation occurs primarily on prior grain boundaries and deformation bands. In the Mn containing alloys, the precipitation occurs on prior grain boundaries and through heterogeneous nucleation on $MnAl_6$ particles. The presence of these heterogeneous nucleation sites accelerates precipitation and increases the volume fraction of precipitates. In the later stages of the TMP particle stimulated nucleation of recrystallization competes with

recovery as the predominate factor governing microstructural evolution.

Mechanical testing results showing moderate superplastic ductilities are consistent with microstructural evidence that the fully processed materials are not fully recrystallized. It should be noted here that the method of microscopy sample collection during the rolling process may have affected the extent of recrystallization. It was necessary that the materials spend brief periods of time (ranging from 30 to 45 seconds) out of the furnace each time a sample was cut. Consequently, some time at temperature was lost. Such a loss would not occur during normal rolling operations. The increase in strain rate sensitivity coefficient at true strains higher than $\varepsilon \approx 0.30$ is a new observation. Explanations for the tendency of m to increase with strain as superplastic flow proceeds beyond the maximum flow stress are not clear.

V. CONCLUSIONS

The conclusions and observations of this research are as follows.

1. The modified TMP schedule provides for superplasticity in the three alloys considered.

2. Microstructural data for the Al-10Mg alloy revealed precipitation on prior grain boundaries and deformation bands in initial stages of the TMP, followed by recovery. There was limited particle stimulated nucleation of recrystallization in the vicinity of large particles.

3. Microstructural data for the Al-10Mg-0.2Mn and Al-10Mg-0.5Mn alloys revealed precipitation on prior grain boundaries and $MnAl_6$ particles in the early stages of the TMP, followed by recovery. Particle stimulated nucleation of recrystallization around large particles and in association with clusters of smaller particles was seen.

4. The presence of $MnAl_6$ particles accelerated precipitation and resulted in a higher volume fraction of particles in the fully processed Mn-containing materials.

5. Although recrystallization was most extensive in the Al-10Mg-0.2 and Al-10Mg-0.5mn alloys, none of the materials achieved a fully recrystallized grain structure by the end of TMP.

6. Strain rate sensitivity coefficients and ductilities increased with the addition of Manganese.

7. The strain rate sensitivity coefficients decreased with increasing strain, consistent with grain growth, during straining up to $\varepsilon = 0.30$. However, beyond this value of strain, m-values unexpectedly increased again. An explanation for this phenomenon is not yet clear.

VI. RECOMMENDATIONS FOR FURTHER RESEARCH

Recommendations for further research are listed below.

1. Time at temperature was lost during TMP to collect samples for microscopy. To fully assess the effect of the rolling schedule on the alloys, rolling should be accomplished without obtaining samples at intermediate stages.

2. Quantitative microstructural analysis should be done to determine volume fraction of precipitates and particle size to assess their impact on microstructural evolution and superplastic response.

3. Tensile testing to strains less than the failure strain is necessary to identify possible microstructural changes during superplastic deformation, and to determine the cause of increasing strain rate sensitivity coefficients at strains above $\varepsilon = 0.30$.

LIST OF REFERENCES

1. Presnyakov, A.A., and Chervykova, V.V., *Proceedings of the Institute of Nuclear Physics,* vol. 2, p. 30, 1959.

2. Underwood, E.E., "A Review of Superplasticity and related Phenomena," *Journal of Metals,* December, 1962.

3. McNelley, T.R., and Kalu, P.N., "The Deformation Mechanisms of Low Temperature Superplasticity in Al-Mg Alloys," *Superplasticity in Advanced Materials,* edited by S. Hori, M. Tokizane, and N. Furushiro, The Japan Society for Research on Superplasticity, 1991.

4. McNelley, T.R., and Stengle, A.F., "The Influence of Thermomechanical Processing Variables on Superplasticity in a High Mg, Al-Mg Alloy," *Metallurgical Transactions,* vol. 17A, June 1986.

5. Hales, S.J., McNelley, T.R., and Crooks, R., "Continuous Recrystallization During Thermomechanical Processing of a Superplastic Al-10Mg-0.1Zr Alloy," *Proceedings of the International Conference on Recrystallization in Metallic Materials,* edited by T. Chandra, The Minerals, Metals & Materials Society, 1990.

6. Sherby, O.D. and Wadsworth, J. "Development and Characterization of Fine-Grain Superplastic Materials," *Deformation, Processing and Structure,* American Society for Metals, 1982.

7. Chawla, K.K. and Meyers, M.A., *Mechanical Metallurgy, Principles and Applications,* Prentice-Hall Inc, Englewood Cliffs, NJ, 1984.

8. Lee, E.W. and McNelley, T.R., "Microstructural Evolution During Processing and Superplastic Flow in a High Mg, Al-Mg Alloy," *Materials Science and Engineering,* vol. 93, pp. 45-55, 1987.

9. McNelley, T.R., Lee, E.W., and Mills, M.E., "Superplasticity in a High Mg, Al-Mg Alloy," *Metallurgical Transactions,* vol. 17A, June 1986.

10. Hales, S.J., McNelley, T.R., and McQueen, H.J., "Recrystallization and superplasticity at 300°C in an Aluminum-Magnesium alloy," *Metallurgical Transactions,* vol. 22A, May 1991.

11. Crooks, R., Kalu, P.N., and McNelley, T.R., "Use of Backscattered Electron Imaging to Characterize Microstructure of a Superplastic Al-10Mg-0.1Zr Alloy," *Scripta Metallurgica,* vol. 25, pp. 1321-1325, 1991.

12. *Metals Handbook,* American Society for Metals, vol. 8, 8th ed., 1973.

13. Gorsuch, T.E., "The Roles of Strain and Reheating Interval in Continuous Recrystallization During the Thermomechanical Processing by Warm Rolling of an Al-Mg Alloy," Master's Thesis, Naval Postgraduate School, Monterey, California.

14. Nes E., "Continuous Recrystallization and Grain Growth During Superplastic Flow," in *Superplasticity,* The International Conference on Superplasticity, edited by B. Baudelet and M. Suery, 1985.

INITIAL DISTRIBUTION LIST

		No. Copies
1.	Defense Technical Information Center Cameron Station Alexandria, Virginia 22304-6145	2
2.	Library, Code 52 Naval Postgraduate School Monterey, California 93943-5002	2
3.	Weapons Systems Engineering Curricular Office Code 33 Naval Postgraduate School Monterey, California 93943	1
4.	Professor T. R. McNelley, Code ME/Mc Department of Mechanical Engineering Naval Postgraduate School Monterey, California 93943	4
5.	Adjunct Professor P. N. Kalu, Code ME/Mc Department of Mechanical Engineering Naval Postgraduate School Monterey, California 93943	1
6.	Adjunct Professor R. Crooks, Code ME/Mc Department of Mechanical Engineering Naval Postgraduate School Monterey, California 93943	1
7.	Dr. Lewis Sloter, Code AIR 931A Headquarters, Naval Air Systems Command Washington D.C. 20361	1
8.	LT Chris D. Meyer 7 LaSalle Drive Decatur, Illinois 62521	1